Expanding heterochromatin reveals discrete subtelomeric domains delimited by chromatin landscape transitions

Antoine Hocher, Myriam Ruault, Petra Kaferle, Marc Descrimes, Mickaël Garnier, Antonin Morillon, Angela Taddei

▶ **To cite this version:**

Antoine Hocher, Myriam Ruault, Petra Kaferle, Marc Descrimes, Mickaël Garnier, et al.. Expanding heterochromatin reveals discrete subtelomeric domains delimited by chromatin landscape transitions. Genome Research, 2018, 28 (12), pp.1867-1881. 10.1101/gr.236554.118 . hal-01977753

HAL Id: hal-01977753

https://hal.sorbonne-universite.fr/hal-01977753

Submitted on 11 Jan 2019

HAL is a multi-disciplinary open access archive for the deposit and dissemination of scientific research documents, whether they are published or not. The documents may come from teaching and research institutions in France or abroad, or from public or private research centers.

L'archive ouverte pluridisciplinaire **HAL**, est destinée au dépôt et à la diffusion de documents scientifiques de niveau recherche, publiés ou non, émanant des établissements d'enseignement et de recherche français ou étrangers, des laboratoires publics ou privés.

Expanding heterochromatin reveals discrete subtelomeric domains delimited by chromatin landscape transitions

Antoine Hocher[1,2], Myriam Ruault[1,2], Petra Kaferle[1,2], Marc Descrimes[1,2], Mickael Garnier[1,2], Antonin Morillon[1,2], Angela Taddei[1,2]

Affiliations:

[1] Institut Curie, PSL Research University, CNRS, UMR3664, F-75005 Paris, France

[2] Sorbonne Université, UPMC Univ Paris 06, CNRS, UMR3664, F-75005 Paris, France

Abstract

The eukaryotic genome is divided into chromosomal domains of heterochromatin and euchromatin. Transcriptionally silent heterochromatin is found at subtelomeric regions, leading to the telomeric position effect (TPE) in yeast fly and human. Heterochromatin generally initiates and spreads from defined loci, and diverse mechanisms prevent the ectopic spread of heterochromatin into euchromatin. Here, we overexpressed the silencing factor Sir3 at varying levels in yeast and found that Sir3 spreads into Extended Silent Domains (ESDs), eventually reaching saturation at subtelomeres. We observed the spread of Sir3 into subtelomeric domains associated with specific histone marks in wild-type cells and stopping at zones of histone mark transitions including H3K79 tri-methylation levels. Our study shows that the conserved H3K79 methyltransferase Dot1 is essential in restricting Sir3 spread beyond ESDs, thus ensuring viability upon overexpression of Sir3. Lastly, our analyses of published data demonstrate how ESDs unveil uncharacterized discrete domains isolating structural and functional subtelomeric features from the rest of the genome. Our work offers a new approach on how to separate subtelomeres from the core chromosome.

Introduction

Heterochromatin classically designates chromosomal domains that remain condensed throughout the cell cycle (Emil Heitz 1928). In contrast to gene specific repressors, heterochromatin silences genes independently of their DNA sequence (Talbert and Henikoff 2006). Heterochromatin is prevalent in eukaryotic genomes and is key to processes including gene dosage compensation, cell differentiation, speciation and genome stability (Grewal and Jia 2007).

Telomeres and a portion of subtelomeres are associated with heterochromatin in many species (Louis and Becker 2014). Subtelomeres are genomic domains that are particularly difficult to define. While they often exhibit structural and functional properties, such as the presence of specific gene families, chromatin marks or a relatively fast gene turnover, there is no strict definition that segregates all these properties between subtelomeres and the core genome (Louis and Becker 2014).

Transcriptional silencing generally initiates at defined loci and propagates by self-recruitment mechanisms (Grunstein 1997; Hoppe et al. 2002; Grewal and Jia 2007; Gartenberg and Smith 2016). The coupling of histone modifying enzymes to nucleosomes allows the specific binding of silencing effectors and drives the formation of heterochromatin domains (Richards and Elgin 2002; Wang et al. 2016). However, the spread of heterochromatin must be limited to prevent encroaching on euchromatin (Donze and Kamakaka 2002).

In budding yeast, the silent information regulator (SIR) proteins, Sir2 Sir3 and Sir4, implement stable repression at the two cryptic mating type loci (*HML and HMR*) and semi-stable repression of genes near telomeres (Gartenberg and Smith 2016; Grunstein and Gasser 2013; Aparicio et al. 1991; Moazed et al. 1997; Rine and Herskowitz 1987; Rudner et al. 2005; Rusche et al. 2003). The SIR complex is recruited at these loci by a combination of specific DNA binding proteins that have functions outside silencing. At telomeres, the Repressor activator Rap1 binds the degenerated telomeric sequence $TG_{1–3}$ (Shampay et al. 1984), and recruits the SIR complex through direct interaction with Sir3 and Sir4. This recruitment is reinforced by additional interactions between Sir4 and the Ku heterodimers (Tsukamoto et al. 1997; Roy et al. 2004)

Once nucleated, the activity of Sir2, a conserved histone deacetylase, creates favorable binding sites for Sir3, which preferentially binds deacetylated H4K16. Iterative cycles of Sir2 mediated histone deacetylation and Sir3 binding allow the self-propagation of the SIR complex on chromatin until a barrier is eventually reached (Grunstein and Gasser 2013; Gartenberg and Smith 2016).

Boundaries restrict silent domains at the cryptic mating type loci (Donze et al. 1999; Donze and Kamakaka 2001). A tRNA gene confines the Sir complex to *HMR* (Donze et al. 1999) while directional nucleation restricts silencing at *HML* (Bi et al. 1999). About half of subtelomeres have a Y' middle repeat isolated from SIR spreading by the transcription factor Reb1. At these subtelomeres, adjacent internal TG repeats associated with the middle repetitive sequence core X can act as relays of silent chromatin propagation (Pryde and Louis, 1999; Fourel et al, 2002: Thurtle and Rine 2014; Ellahi 2015). Beyond these last nucleation sites, the spread of silencing is rather limited ranging from hundreds of base pairs to few kb and no boundary has been identified so far. However, Sir3 was recently shown to expend inward chromosomes in G1 arrested cells (Mitsumori et al. 2016). Although numerous factors such as nuclear pore complex components and transcription factors

display barrier properties in boundary assays, their physiological role *in vivo* remains to be explored (Oki et al. 2004). The collective action of chromatin modifying enzymes implements chromatin states that potentially decrease Sir3 affinity for nucleosomes. In addition to the acetylation of H4K16 by the SAS-I complex, acetylation of histone H3 tails by Gcn5 and Elp3, methylation of H3K4 and H3K79, and H4K16ac-dependent incorporation of the H2A.Z histone variant were all proposed to contribute to limit Sir3 spreading at subtelomeres (Gartenberg and Smith 2016). In mutants lacking those enzymes or marks the SIR complex propagates further away from the telomeres (Suka et al. 2002; Sperling and Grunstein 2009; Kristjuhan et al. 2003; Meneghini et al. 2003). However, the respective contribution of each mechanism to heterochromatin restriction and what further limits the spread of silencing in those mutants remains unknown.

A key parameter regulating heterochromatin dynamics, function and spatial distribution is the concentration of silencing factors. For instance, increasing Sir3 dosage in budding yeast expands subtelomeric silent domains toward the chromosome core (Renauld et al. 1993a) and increases telomere clustering (Ruault et al. 2011). However, extension of silencing domains was monitored at few subtelomeres and the dose-dependency of heterochromatin propagation remains qualitative (Renauld et al. 1993a; Hecht et al. 1996; Strahl-Bolsinger et al. 1997; Katan-Khaykovich and Struhl 2005). Here we examine the impact of expressing the silencing factor Sir3 at varying levels genome-wide.

Results

Saturation of extended silent domains upon *SIR3* overexpression

To systematically examine the impact of elevated Sir3 on the genome, we generated yeast strains that overexpress *SIR3* at stable, different and non-overlapping levels. We replaced the endogenous *SIR3* promoter with three different promoters, generating strains that produced 9×-Sir3 (*pscADH1-SIR3*, hereafter denominated "*pADH-SIR3*"), 16×-Sir3 (*pscTEF1-SIR3*, "*pTEF-SIR3*"), and 29×-Sir3 (*pscTDH3-SIR3, "pGPD-SIR3"*) as determined by Western blot (Fig S1A), and fluorescence quantification of live cells expressing Sir3-GFP (Fig 1A, Fig S1B). FACS profiles of wild-type and *pGPD-SIR3* strains were largely similar, suggesting that the cell cycle was unaffected by overexpression of *SIR3* (Fig S1C).

We probed genome-wide Sir3 binding by ChIP-chip using our antibody raised against the full-length native (untagged) protein (Ruault et al. 2011).We obtained a high signal to noise ratio (above 300) in the vicinity of known nucleation sites, namely TG repeats, ARS consensus sequence of the X-core elements (ACS) and the two cryptic mating type loci, in agreement with previous studies (Ellahi et al. 2015; Teytelman et al. 2013; Radman-Livaja et al. 2011; Sperling and Grunstein 2009). To rule out potentially confounding effects due to well documented ChIP artifacts, we compared the binding of Sir3 within subtelomeres to its binding at highly transcribed genes, a known source of artefactual signal (Teytelman et al. 2013; Park et al. 2013; Kasinathan et al. 2014). Finally, we compared Sir3 binding to that of the chromatin binding deficient mutant Sir3-A2Q as an additional control. In both cases, the signature of hyper-chipable loci was negligible compared to Sir3 binding signal at subtelomeres (Fig S1D, S1F), providing confidence in the integrity of our data.

On average in wild-type cells, we detected Sir3 binding up to 2,6 kb away from the last telomeric element (ACS), with some weaker signal at sites previously reported as secondary nucleation sites, consistent with previous studies (Lieb et al. 2001; Sperling and Grunstein 2009; Ellahi et al. 2015; Radman-Livaja et al. 2011). Elevation of Sir3 levels expanded the distance of Sir3 binding to ~12 kb in 9×Sir3 cells and up to ~19 kb in 16× or 29×Sir3 cells (Fig 1B). Sir3 spreading was similar in 16× and 29×Sir3 cells. Sir3-GFP nuclear background levels almost doubled in 29×Sir3 compared to 16×Sir3 cells (Fig S1E), arguing that Sir3 binding to chromatin reached saturation. The constitutive overexpression of Sir3 submerged most of the secondary recruitment sites that were present in wild-type cells leading to the formation of extended continuous Sir3 bound domains at most subtelomeres. We observed that Sir3 binding increased at few euchromatic (non subtelomeric) sites upon Sir3 overexpression such as *YAT1* or *YFR017W* (Fig S1F and table S1) but chose not to pursue this further as in most cases changes in Sir3 binding were not associated with changes in gene expression in agreement with previous reports (Marchfelder et al. 2003).

In parallel, we monitored telomere foci in function of Sir3 concentration by live microscopy imaging of Rap1-GFP (Fig 1C-E). In wild type cells, telomeres cluster together in 3 to 5 foci located at the nuclear periphery (Gotta et al. 1996). However, upon Sir3 overexpression using the *Gal1p* promoter, most of the telomeres group together in the center of the nucleus (Ruault et al. 2011a). In the range of Sir3 concentration probed, we observed that telomere clustering increased non-linearly as a function of Sir3 levels and this reached saturation at levels between 9-16×Sir3. Most cells (78%) had at least 3 Rap1-GFP foci in the WT strain while 64-76% of cell had one or two foci in strains overexpressing Sir3 9-fold or more (Fig 1D). Increased foci intensity paralleled the decrease in foci number (Fig 1E, Left), consistent with increased telomere grouping in cells overexpressing Sir3. Furthermore, the

proportion of nuclear Rap1-GFP within foci increases from 13.6% in *WT* cells to a maximum of 21.6-22.2 % for Sir3 dosage above 16-fold (Fig 1E, Right). Together, this suggests that not all telomeres are clustered within Rap1 foci in *WT* cells at a given time, and that elevated Sir3 levels increase the total number of telomeres within clusters, a process eventually reaching saturation. Thus, increased Sir3 dosage expands Sir3 genome binding and telomere clustering until they reach saturation between 9-16×Sir3.
However, individual telomeres showed different stereotypical behaviours in response to increased Sir3 dosage. We classified telomeres based on their response to Sir3 dosage elevation (see Methods). One example of each class is displayed on (Fig 1F) and full data is shown on (Fig S1G). "Fragile" subtelomeres (6/26) displayed increased Sir3 spreading and plateaued at 9×Sir3. "Progressive" subtelomeres (13/26) displayed gradually increased Sir3 spreading between 9-16×Sir3 and then plateaued at 16×Sir3. "Resistant" subtelomeres (4/26) displayed increased Sir3 spreading and plateaued at 16×Sir3. Finally, "insensitive" subtelomeres (3/26) did not expand in response to elevated Sir3 levels. The expanded Sir3 domains showed diverse lengths in all categories, ranging from 7-25 kb (*HM* excluded), independently of chromosomal arm length or middle repeat content (Fig S1H-I).

Sir3 spreading extends Silent Domains

Overexpression of *SIR3* repressed subtelomeric transcription, as expected. Given that overexpression of the point mutant *sir3-A2Q*, which leads to telomere clustering but only binds to telomeric repeats (Fig 2A-B), did not affect global transcription of subtelomeres (Fig S2A), repression was attributed to Sir3 binding to chromatin and not clustering of telomeres. However, 22 genes showed transcriptional changes common to the overexpression of *SIR3-A2Q* and *SIR3*, *i.e* potentially caused by telomere clustering, including 20 euchromatic genes (Fig S2D). Those transcriptional changes could be the consequences of changes in spatial localization or alternatively due to the sequestering of specific factors within the telomere hyper-clusters.

The extension of Sir3-bound domains upon *SIR3* overexpression systematically repressed underlying transcripts genome-wide (Fig 2C for the *Tel6R* and 2D genome wide) providing a parallel assessment of the validity of binding events measured by ChIP-chip. Repression was largely independent of initial transcript level (Fig 2D) and of coding status (e.g. the right subtelomere of Chromosome VI, Fig 2C, Fig S2B). These extended silent domains (ESDs) included 100 genes that were not bound by Sir3 in *WT* cells. The logarithm of transcriptional repression was linearly proportional (R^2=0.71) to the Sir3 binding signal, reflecting the absence of silencing escapers (Fig 2D). Analysis of reads mapping to multiple loci indicated that entire gene families, characteristic of subtelomeres and Y' elements, were on average repressed upon *SIR3* overexpression (Fig S2C, S2E), suggesting that the subtelomeric regions devoid of chip probes are collectively silenced within ESDs.

Most genes within ESDs are not highly transcribed in *WT* cells, suggesting that Sir3 spreading might be limited by transcription. However, highly expressed genes like *IRC7* (Fig 2C) and *DLD3* (Fig 3B) were not excluded from ESDs and were repressed upon *SIR3* overexpression. Both genes belong to the top 10% of most expressed genes and to the top 20% of most frequently transcribed genes in wild-type cells (Pelechano et al. 2010). Similarly, at 7 subtelomeres at least one gene within the ESD had higher read density than the gene adjacent to the ESD (Fig 2E). Furthermore, genes found immediately before and after the

end of ESDs showed comparable transcript levels (Fig 2F). Therefore, transcriptional activity *per se* did not appear sufficient to limit Sir3 spreading when Sir3 is over-abundant.

The limitation of Sir3 spreading could be the consequence of the counter selection of cells silencing essential genes as ESDs did not contain any and 3 ESDs ended right before three essential genes. However, we do not favour this hypothesis for two main reasons. First, we did not detect significant decreases in mRNA levels for these genes upon Sir3 overexpression. Second, none of these genes show any haplo-insufficiency phenotype (Deutschbauer et al. 2005) arguing that a weak repression would likely not be counter-selected. We thus conclude that extended Sir3 spreading led to efficient gene silencing of the underlying genes and that gene activity did not account for the end of ESDs.

ESDs are not limited by distance from the telomere or by barrier TF elements

To test whether the distance from the telomere limits Sir3 spreading, we compared Sir3 spreading at a *WT* telomere *VIIL* against a 15 kb truncated version (Fig 3A). In both cases, Sir3 binding ended within the *HXK2* promoter, with a somewhat sharper decline rate in the truncated strain. This suggests that the Sir3 spreading boundary is either defined relative to the chromosome core or is a local feature. Focusing on silent domain ends, we quantified the slope of Sir3 binding at each subtelomere in the strains overexpressing *SIR3*, when sufficient data were available (24/32 subtelomeres). We found that the slope at the end of a silent domain did not correlate with the distance from the telomere (*i.e* nucleation point) and there was no correlation with the groups defined based on sensitivity to Sir3 dosage (Fig S3A). Thus, when Sir3 is in excess, the delineation of the ESD did not depend on the distance from the nucleation site. To investigate whether DNA sequence-specific barrier elements confine Sir3 ESDs within subtelomeres, we evaluated the available binding data of 10 transcription factors (TF) with proposed barrier activity (Adr1, Gcn4, Rgt1, Hsf1, Sfp1, Reb1, Abf1, Leu3, Swi5: (Harbison et al. 2004), Rap1: (Rhee and Pugh 2012),Tbf1: (Preti et al. 2010)). At 12 subtelomeres, we identified bound TF sites at genes corresponding to the ESD limit (Fig S3C). However, each of these TFs was also bound elsewhere within the ESD (Fig 3B) indicating that they were not sufficient to limit the spreading of Sir3. Only the three subtelomeres categorized as insensitive to Sir3 levels (group 4), contained known barrier elements flanking Sir3 bound domains: a *tRNA* gene at subtelomere *IIL*, a previously identified barrier sequence homologous to the left barrier of *HML* (Bi 2002) at the subtelomere *XIR* and the I silencer at subtelomere *IIIL* (Fig S3B). Thus, in most cases, none of the previously identified barrier elements that we could probe was sufficient to block Sir3 spreading.

Sir2 does not limit the majority of extended silent domains

We considered that Sir3 spreading might be limited by the capacity of Sir2 to deacetylate H4K16. We first monitored the genome-wide occupancy of Sir3 in strains overexpressing Sir2. We found that Sir2 overexpression had a weaker impact than 9×Sir3 overexpression (Fig S4A). Sir3 spreading in cells co-overexpressing Sir2 and Sir3 or overexpressing Sir3 alone were identical at most subtelomeres (19/26), as illustrated by their mean ChIP profile (Fig 4A). In the remaining 7 cases Sir3 spreading was increased by co-overexpression of Sir2, slightly extending the average profile of Sir3 binding (Fig S4B). It is noteworthy that the further extended silent domains remained devoid of essential or tRNA genes. Thus, Sir2 activity did not generally limit the spread of heterochromatin, even when Sir3 is in excess.

ESDs encompass known domains of Sir3 extension

We compared how Sir3 bound domains extend upon overexpression to known situations of Sir3 binding extension: Sir3 spreading in H3 tail mutants (Sperling and Grunstein 2009) and in cells blocked in G1 by alpha-factor treatment (Mitsumori et al. 2016). As shown on Fig 4, ESDs encompass the domains bound by Sir3 in H3 tail mutants or in G1 blocked cells. Although in the H3 tail mutant Sir3 bound domains increased only at half subtelomeres, in these cases Sir3 binding profiles were very similar to those observed upon *SIR3* overexpression (Fig 4B and Fig S4B). In contrast, Sir3 binding in G1 blocked cells appeared to cover domains identical to ESDs but with a binding signature qualitatively different, as only a low magnitude binding signal is observed in the extended Sir3 binding domains.

Together, this shows that Sir3 bound domains in G1 blocked cells or in *H3Δ4-30* are contained within ESDs, although Sir3 is not overexpressed in these conditions. This suggests that the same determinants of Sir3 restriction are at play in all these contexts. Finally, the similarities of Sir3-bound domains in those conditions may indicate that ESDs correspond to chromosomal features that exist independently of Sir3 dosage.

ESDs coincide with a pre-existing chromatin landscape

To identify potential chromatin determinants of ESDs, we analyzed the genome-wide distribution of 27 histone marks or variants (Weiner et al. 2015; Schulze et al. 2009). We first computed the correlation between Sir3 binding signals and histone modifications across the first centromere proximal 50 kb flanking X-core elements (Fig 5A). Consistent with previous results, we observed the expected anti-correlation between Sir3 binding and H4K16 acetylation in *WT* cells with a Pearson correlation coefficient of -0.45 (Fig 5A, and exemplified in Fig 5B). Correlation between Sir3-A2Q binding and histone marks ranged from -0.25 to 0.2, providing a negative control. Generally, in wild-type cells Sir3-bound nucleosomes were depleted of most histone marks, with the exception of H4R3 methylation and H2A phosphorylation, which were enriched within silent domains (Fig S5A), as reported earlier (Yu et al. 2006; Szilard et al. 2010). We observed that Sir3 binding signal was better correlated with several histone marks in all conditions corresponding to extended binding of Sir3 (H3 tail mutants, G1 blocked cells, *SIR3* overexpression and *SIR2* and *SIR3* co-overexpression) than in asynchronous wild-type cells. Namely, Sir3 binding signal correlated better with histone H3 methylation and histone H2A phosphorylation (Fig 5A, B), the highest correlation values being with Sir3 binding signal in cells co-overexpressing *SIR2* and *SIR3* (Pearson correlation coefficient of -0.49 with H3K79me3 and 0.72 with H2AP). While Sir3 binding in G1 blocked cells remained negatively correlated with H4K16 acetylation status, this anti-correlation was much weaker in H3 tail mutants and even lower in strains overexpressing *SIR3*. This suggests that H4K16 acetylation might limit Sir3 binding in G1 blocked cells but not in H3 tail mutants or upon *SIR3* overexpression.

To investigate a potential link between chromatin and the consequences of *SIR3* overexpression, we compared histone marks enrichment at the flanks of wild type silent domains among the fragile, progressive and robust subtelomere groups defined in Fig 1. We observed that some histones marks are on average differentially enriched in the three groups (Fig S5A). The most pronounced differences (Kruskal-Wallis, p-val < 10^{-4}) concerned H3K79me2 and the acetylation of the H4 tail lysines (K5,8,12 but not K16: ANOVA, p-val = 0.55) that showed higher levels within ESDs of progressive telomeres than at fragile telomeres and even higher levels at robust telomeres.

As acetylation of H4K5,8,12 reduces Sir3 affinity for H4 in a cumulative manner (Carmen et al. 2002), those differences could contribute to the differential spreading observed between

those groups of subtelomeres upon overexpression of *SIR3*. Similarly, Sir3 H3K79me2 could limit Sir3 spreading at progressive and robust telomeres when Sir3 is overexpressed 9-fold but not above.
H3K79me, and the histone variant H2A.Z, previously reported as antagonistic to SIR spreading, showed low levels in wild type silent domains similar to the bulk of the genome but were enriched within the ESDs and returned to background levels past ESDs (Fig 5A, C). This suggested that these chromatin features did not efficiently block Sir3 spreading when Sir3 is over-abundant or in G1 phase.

In contrast, H3K4me3, H3K36me3 and H3K79me3 were only present after the ESD terminus (Fig 5C, S5B). We reasoned that the longer intergenes present within subtelomeres might bias our analysis, artificially leading to the depletion of marks associated to gene bodies. To control for this potential artifact, we separated promoter nucleosomes (-3, -2, -1) from gene body nucleosomes and obtained essentially the same results (Fig S5C).

Thus, the subtelomeric chromatin landscape exhibits more similarities with Sir3 binding when it is extended than with Sir3 bound region in wild-type asynchronous population.

In a complementary approach, we focused on Sir3 binding signal at the ends of ESDs. We classified each subtelomere according to Sir3 binding signal's area under the curve (AUC), computed on the logistic-like fit of the Sir3 binding signal in ESDs (see Methods). At the ten telomeres showing the highest AUC, some histone marks displayed sharp transitions, particularly H3K79me3 and H2AS129P (Fig 6A). In contrast, the ten subtelomeres with the lowest Sir3 binding AUC at ESD ends showed rather smooth changes both for Sir3 binding and for these marks (Fig 6A and S6A). Thus, ESDs correlated with a pre-existing chromatin landscape defined by specific histone modifications, low levels of H3K79me3 and H3K36me3 and high levels of H2AP.

The methyl transferase Dot1 is essential for viability when *SIR3* is overexpressed.
As H3K79 methylation has been shown to impair the binding of Sir3 to histone peptides and to nucleosome *in vitro* (Altaf et al. 2007; Wang et al. 2013), it appeared as a good candidate to limit ESDs. To test this hypothesis, we overexpressed *SIR3* in this absence of Dot1, the only methyltransferase responsible for H3K79 mono-, di- and tri-methylation. We found that the *dot1Δ GPD-SIR3* strains were sick and generated suppressors upon streaking. To avoid artifacts due to these potential escapers, we selected *dot1Δ GPD-SIR3* clones in the presence of 5 mM nicotinamide (NAM), which inhibits Sir2 activity and thus silencing (Bitterman et al. 2002). After the selection of positive clones, we assessed the growth of these mutants on medium without NAM, allowing silencing to initiate (Osborne et al. 2009). Above 9-fold overexpression of *SIR3*, *dot1Δ* mutants exhibited growth defects that were proportional to Sir3 amounts and rescued by Sir2 inhibition (Fig 6B). In contrast, the H3K4 and H3K36 methyltransferases Set1 and Set2, and the histone deacetylase Rpd3 were all dispensable to maintain cell growth in presence of high Sir3 dosage (Fig S6B). A *dot1Δ* strain overexpressing the spreading-defective *Sir3-A2Q* point mutant was viable, further supporting that the requirement for Dot1 is to restrict the spread of Sir3 and not the clustering of telomeres (Fig S6B). Furthermore, co-overexpression of *DOT1* and *SIR3* led to loss of silencing, showing that H3K79 methylation prevails on Sir3 binding even when *SIR3* is overexpressed (Fig S6C).

H3K79 methylation protects euchromatin from the spread of silencing
To identify H3 and H4 histone residues involved in the limitation of Sir3 spreading, we set a genetic screen based on the Synthetic Gene Array (Dai and Boeke 2012). *H3K79R* was the

sole histone point mutant having growth defects that could be rescued by 5 mM NAM treatment (Fig 6C, S6D) indicating that H3K79 methylation plays a key role in limiting Sir3 spreading. In contrast, the *H4K16R* mutant had non-significant growth defects (Fig 6C, S6E), consistent with a rather subtle influence of H4K16 on the maximal extent of silencing upon *SIR3* overexpression.

Next, we observed Sir3 binding events that led to cell lethality in *DOT1* deleted mutants overexpressing *SIR3*. To do so, cells were first grown in the presence of NAM, and then released into fresh medium for 8 hours. Sir3 binding in cells overexpressing *SIR3* released from NAM was very similar to what we observed in cells grown in the absence of NAM (Pearson correlation coefficient, 0.9). In contrast, in *dot1Δ* mutants overexpressing *SIR3,* Sir3 spread beyond ESDs at several subtelomeres and bound numerous euchromatic sites (Fig 6D, E). The subtelomeric extension of Sir3 spreading encompassed 4 essential genes as shown for subtelomeres 3L, 3R and 2L (Fig 6D and S6E) likely accounting for the lethality of this strain. In addition, Sir3 overcame the three previously identified barriers including the tRNA gene present at the border of subtelomere 2L that was insensitive to Sir2 and Sir3 overexpression in otherwise wild-type cells (Fig S6E).
To define the inhibitory effect of each H3K79 methylation state on Sir3 binding, we compared Sir3 binding in *dot1* mutants overexpressing *SIR3* to the levels of mono, di and tri-methylation of H3K79 deposited by Dot1 in WT cells. We observed that in the absence of Dot1, Sir3 was binding loci that were enriched for H3K79 tri-methylation but depleted for H3K79 mono-and di-methylation in wild type cells (Fig 6F). This suggests that it was the tri-methyl state of H3K79 that inhibited Sir3 binding and so prevented heterochromatin formation within euchromatin.
Accordingly, *SIR3* overexpression was also lethal in *rad6Δ* cells (Fig S6F), these lack H3K4me3 and H3K79me3 but not H3K79me1 and 2 (Ng et al. 2002; Schulze et al. 2009). We thus conclude that H3K79me1 and me2 could contribute to but are not sufficient for blocking Sir3 binding within euchromatin.

ESDs coincide with discrete domains that segregate subtelomeric features.

We identified discrete subtelomeric domains corresponding to the maximal extension of Sir3 bound domains. We next sought to identify regulators of genes found in these domains by screening a compendium of over 700 mutants (Kemmeren et al. 2014). We classified subtelomeric genes into four different groups (1) genes or pseudo-genes associated with middle repeat elements (telomeric), (2) genes bound by Sir3 in *WT* cells, (3) genes bound by Sir3 only upon *SIR3* overexpression and (4) genes bound Sir3 only upon co-overexpression of *SIR2* and *SIR3*. Groups 3 and 4 correspond to ESDs. We also considered the group of genes located within 10 kb from the end of ESDs and located between 10-20 kb from ESD ends as a control.

For each mutant, we tested if the proportion of differentially expressed genes ($|\log_2(FC)|>2$) within a subtelomeric domain was higher than expected by chance, considering the effect of each mutation on the rest of the genome. We identified genes whose mutation affects specific subtelomeric subdomains (Fig 7A). As expected, deletion of any of the *SIR* had localized effects within the telomeric and WT Sir3 bound domains.

Our analysis confirmed mutants previously known to affect subtelomeric transcription. Telomerase components and the nucleoporin *NUP170* (Van De Vosse et al. 2013) up regulates specifically the most telomeric group of genes in our analysis, while the mediator

complex tails proteins Med2, Med15 and Gal11 (Peng and Zhou 2012; Lenstra et al. 2011), the Hda1/2/3 complex, and the general repressors Tup1/Cyc8 specifically affect genes located within ESDs (Fig 7A). Importantly, the localized enrichment for downregulated genes in *rpd3* or *sas2/4/5* mutants did not extend beyond the ESDs. This enrichment for downregulated genes was likely the consequence of increased spreading of the SIRs in those mutants. Therefore, SIR dependent silencing in those mutants seemed not to extend beyond ESDs, further reinforcing the notion that ESDs represent the maximal extension of SIR dependent silencing. Lastly, enrichment for downregulated genes in the *tup1 and Ssn6* mutants decreased abruptly at the end of ESDs (Fig S7A-B) and no mutant had enriched impact on the genes in the 10 kb immediately adjacent to ESDs. Thus, the domains defined by the saturated expansion of silent chromatin encompassed the subtelomeric domains in which known mutants affecting subtelomeres have an effect.

Lastly we probed how the ESD point of view segregates subtelomeric properties as compared to other definitions of subtelomeres: distance from telomeres, from the first essential gene, the end of HAST domains (defined as Hda1 affected subtelomeric regions, (Robyr et al. 2002) or subtelomeres based on synteny conservation across close relative species (Yue et al. 2017). ESDs often extended within the core chromosome as defined by synteny, more than 10 kb at five subtelomeres (Fig S7C), showing that ESD constituted a different definition of subtelomeres. ESD and HAST domains ended at similar location at 8 subtelomeres (<3 kb) but HAST domains, which are only defined at 22 subtelomeres, generally extended beyond ESD (Fig S7D). Furthermore, the transitions of the H2AS129ph and H3K79me3 histone marks (Fig 7B) are evidently sharper from the ESD end viewpoint than from the distance from X-core sequence or syntenically defined subtelomere end. Quantification of H3K79me3 transition by systematic fitting of a linear model around the transition zones confirmed that ESDs better captures H3K79me3 subtelomere to euchromatic transitions than syntenically derived subtelomere or HAST domain ends (Fig 7C). Similar quantification for H2S129P transition showed than ESDs and HASTs comparably segregated H2AS129P although ESDs included four more subtelomeres, both viewpoints being more efficient than syntenically defined subtelomere ends (Fig S7E). Thus, probing the maximal extent of silencing domains revealed discrete subtelomeric domains delimited by histone mark transition zones and provides a new definition of subtelomeres (Fig 7D).

Discussion

The Sir complex has been a model for chromatin complex propagation and gene silencing for decades. Pioneer studies demonstrated that increasing the dose of Sir3 extends silenced domains at subtelomeres (Renauld et al. 1993b; Pryde and Louis 1999), a property common to several heterochromatin complexes. However there has been controversy on the generality of this finding at natural telomeres (Pryde and Louis 1999; Ellahi et al. 2015), and the details of this process remain unclear. Here, we systematically studied the impact of increasing Sir2 and Sir3 dosage on the propagation of the SIR complex and on genome-wide transcription.

Gradual overexpression of Sir3 revealed that the spreading of Sir3 over subtelomeres reached saturation at Sir3 levels between 9 and 16× suggesting the existence of fixed borders. Similarly, telomere clustering increased at 9× and 16× Sir3 levels but not above. Yet, the change in chromosome organization imposed by telomere hyperclustering in the center of the nucleus (Ruault et al. 2011) had a very minor impact on gene expression *per se* as shown by overexpression of the silencing deficient *sir3-A2Q* point mutant. Conversely, spreading of wild-type Sir3 was systematically associated with decreased transcript levels of the underlying genes. This is in contrast with the situation observed in wild-type cells where Sir3 is found at rather discrete loci close to nucleation sites and with a limited effect on gene expression as previously reported (Thurtle and Rine, 2014; Takahashi, 2011). Thus, although Sir3 spreading and impact on gene expression appears limited in laboratory strains and under standardized growth conditions it has the potential to spread over several kb creating domains of silent chromatin that we named ESDs for extended silent domains. Unexpectedly, the response to increase in Sir3 levels differed among subtelomeres, and the concentration of Sir3 required for maximal spreading varied. Additional spreading extended up to 30 kb in-between subtelomeres, independently of middle repeat elements or chromosomal arm length and expression levels of the underlying genes. However, the domains covered by Sir3 upon overexpression shared similar chromatin marks, suggesting that the chromatin landscape dictated the extent of Sir3 spreading. Indeed, we identified H3K79me3 as the most efficient barrier to prevent heterochromatin propagation. Finally, by revealing the maximal subtelomeric domains accessible to Sir complex in viable cells, our work uncovered previously unknown, discrete subtelomeric domains that isolated the structural and functional features associated with subtelomeres.

Different categories of Sir chromatin antagonism

Although our data suggest the existence of fixed borders, our search for punctual barrier elements did not retrieve convincing candidates. Furthermore, native binding sites for transcription factors that block silencing when tethered to chromatin (Oki et al. 2004) were not efficient barriers to Sir3 spreading. We also observed extension of Sir3 binding within regions that were enriched with chromatin marks previously reported as antagonistic to its spreading, such as histone variant H2A.Z (Guillemette et al. 2005; Martins-Taylor et al. 2011; Meneghini et al. 2003) and mono-methylated H3K79 (Altaf et al. 2007). Histone tail acetylation appears to limit spreading of Sir3 when Sir3 is present in a limiting amount. Indeed, we observed that acetylation levels of H4K5,8,12 are higher within ESDs that resist to intermediate levels of *SIR3* overexpression than at other ESDs. Furthermore, H3 tail mutants show increase Sir3 spreading at some subtelomeres within ESDs (Fig 4). Consequently, our work indicates that histone tail acetylation, H2A.Z, and specific transcription factors likely buffer the spread of the SIR rather than block it (Fig 7D).

End of extended silent domains: the specific role of Dot1

We observed that the end of extended silent domains coincides with a major histone mark transition zone, characterized by an increased enrichment of H3K4me3, H3K36me3 and H3K79me3. Deletion of *SET1* or *SET2,* the genes encoding the enzymes responsible for the H3K4me3 and H3K36me3, respectively, had no impact on cell growth upon Sir3 overexpression. In contrast, deletion of *DOT1*, which encodes the only H3K79 methyltransferase in budding yeast, was lethal in this condition. Yet viability in this strain could be rescued by inhibiting Sir2 indicating that loss of H3K79 methylation was responsible for the deadly spreading of elevated Sir3 in the absence of Dot1. Accordingly, when *dot1Δ* strain overexpressing *SIR3* were released from Sir2 inhibitor, Sir3 spread beyond ESDs invading 4 essential genes. In these conditions, Sir3 was also binding numerous euchromatic sites that were enriched for H3K79me3 (but not H3K79me1 or 2) in wild-type cells. H3K79me3 is anti-correlated with H4K5,8 and 12 acetylation (Weiner et al. 2015), which also have the potential to limit Sir3 spreading (Carmen et al, 2002 and above). This suggests that H3K79me3 was protecting nucleosomes hypoacetylated on H4K5,8 and 12 from Sir3 binding at euchromatic sites.

As Dot1 is responsible for mono-, di- and tri-methylation of H3K79 (Stulemeijer et al. 2015) this raises the question of the relative contribution of these marks for blocking Sir3 spreading. *In vitro,* all three H3K79 methyl marks reduce Sir3 affinity for reconstituted nucleosomes (Behrouzi et al. 2016; Martino et al. 2009).

Here we show that upon overexpression, Sir3 spread over domains enriched for H3K79me1 and me2, implying that these marks did not block Sir3 spreading *in vivo* although they slow down silencing establishment (Katan-Khaykovich and Struhl 2005; Osborne et al. 2009). In contrast, H3K79me3 signal increases abruptly where Sir3 spreading stopped. In the absence of Dot1 and upon overexpression of *SIR3*, we observed that Sir3 predominantly binds loci that were initially enriched for H3K79 tri-methylation state. Accordingly, mutants in which H3K79me3 is abolished but not H3H79me and H3K79me2 (Ng et al. 2002; Schulze et al. 2009) were sensitive to *SIR3* overexpression. This is consistent with the observation that Sir3 associate with H3K79 mono and di methylation at an active subtelomeric reporter gene *in vivo* (Kitada et al. 2012). This is also in good agreement with crystal structure data predicting that the potential of H3K79 to form hydrogen bonds with the BAH domain of Sir3 would progressively decrease with H3K79 methylation to be abolished by H3K79me3, thereby decreasing Sir3 affinity to nucleosomes (Armache et al. 2011; Arnaudo et al. 2013).

All together our work demonstrates that H3K79 methylation, predominantly the tri-methyl state, restricts silencing within subtelomeric regions thus protecting euchromatin. As the occupancy of this mark is independent of transcription rate (Schulze et al. 2009), this offers the attractive possibility of preventing heterochromatin spreading independently of transcription.

Subtelomeric specificities

In most organisms, specific features of chromosome ends extend beyond telomeres, within domains generally referred to as subtelomeres (Louis and Becker 2014). In budding yeast, several viewpoints enable the identification of diverse subtelomeric features including a lower gene density, and a faster evolution than the core genome (Yue et al. 2017).

The chromatin landscape also exhibits specific features within domains located proximal to chromosome ends (Matsuda et al. 2015; Millar and Grunstein 2006; Robyr et al. 2002). The

first is undoubtedly the presence of heterochromatin, which has a unique signature in terms of histone marks. However, specific properties associated with chromosome ends often extend beyond heterochromatic domains (Matsuda et al. 2015; Millar and Grunstein 2006). At most *S.cerevisae* subtelomeres, Hda1-affected subtelomeric (HAST) domains (Robyr et al. 2002) and Htz1 activated (HZAD) domains (Guillemette et al. 2005) lie contiguous to SIR silenced chromatin. In addition, phosphorylation of H2AS129 and monomethylation of H3K79 also extend further away than SIR silenced domains. Here we show that ESDs possess a consistent chromatin signature. Namely these domains are enriched for H2AP, Htz1 and depleted of tri-methylated histone H3 which levels show sharp transition at the end of ESDs. Consistently, Htz1 sensitive genes are enriched in these domains. Furthermore, considering the end of ESDs as a boundary between subtelomeres and the core genome segregates genes sensitive to the depletion of chromatin modifiers such as Hda1, Tup1/Ssn6 or Sas2 better than other definitions of subtelomeres (Fig S7D, S7E). Similarly, ESDs segregated transition of histone marks such as H3K73me3 better than other definitions of subtelomeric domains. Thus, ESDs coincide with discrete subtelomeric domains isolating structural and functional features and could provide an alternative definition of subtelomeres. Furthermore, domains defined by ESD contain genes than can collectively be repressed in non-stressful conditions, a notion consistent with the idea that subtelomeres contain genes required for response to stressful environments (Louis and Becker 2014).

At most subtelomeres that we could analyse ESDs are broader or coincide with subtelomeres defined based on synteny conservation across related species (Fig S7A). We and others recently showed that chromatin states impact on efficiency and outcome of both homologous recombination and nucleotide excision repair (Guintini et al. 2017; Batté et al. 2017). This raises the question of whether the specific chromatin state associated with subtelomeric domains uncovered in this study contributes to the particular evolution of those regions.

Contribution of telomere proximity to subtelomeric properties

A central question in the biology of subtelomeres is to what extent the properties of subtelomeres are due to their proximity to telomeres or a mere consequence of their gene content? Several studies demonstrated that the SIR complex contributes to the localization of enzymes to subtelomeres. For example, subtelomeric localization of the Okazaki fragment processing protein Dna2 is severely reduced in sir mutants (Choe et al. 2002). In addition, the kinase Tel1 responsible for H2A phosphorylation in subtelomeric regions is present at telomeres but H2AP levels depend mainly on the integrity of the SIR complex (Kitada et al. 2011). Regions enriched for H2AP coincide with ESDs suggesting that either Sir3 acts remotely, or binds these regions at least transiently in wild-type. Accordingly, profiling of Sir3 binding in G1 arrested cells showed low levels of Sir3 binding within ESDs (Mitsumori et al. 2016). Thus, Sir3 might influence the chromatin landscape in subtelomeric regions. How the transient presence of Sir3 during the G1 phase of the cell cycle could stabilize H2A phosphorylation is unclear. One attracting possibility is that Sir3 acts by recruiting a so far unidentified factor that would remain associated to chromatin through the whole cell cycle.

Conclusion

By taking the opposite approach to depletion studies, our work describes the dose dependency of budding yeast heterochromatin. In the presence of a large excess of silencing factors, ectopic nucleation of heterochromatin remains limited and does not impact euchromatic transcription. In contrast, we observed the extension of subtelomeric silent

domains and characterized their maximal extension along with the antagonistic factors that have been overcome, such as H2A.Z or H3K79me. By scanning chromatin properties associated with Sir3 maximal binding, we uncovered major subtelomeric histone mark transition zones that functionally protect euchromatin from the spread of silencing. The long-term contribution of heterochromatin to the peculiar properties of subtelomeres will require further study.

Methods

Media and Growth conditions

The strains used in this study are listed in Table S2. Yeast cells were grown on YP with 2% glucose, raffinose or galactose. Unless notified, all the strains used in this study were grown at 30 °C with shaking at 250rpm.

Yeast transformation protocol

Cells were seeded on liquid medium and grown to $0,8<OD_{600}<1,2$. 3 ODs (~$3x10^7$ yeast cells) of cells were taken and washed with 1× TEL (10 mM EDTA pH 8, 100 mM Tris pH8, 1M Lithium Acetate), then 3µl of SSDNA (Sigma ref: D9156-5ML), DNA template (0,5µl if plasmid DNA, 5µl of digested plasmid or PCR product), 300µl of 1× TEL and 45% PEG-4000 solution were added. The mix was put 30 min at 30 °C and heat shocked at 42°c for 15 minutes. Lastly, cells were plated on appropriate selective medium.

Rap1 foci analysis

The image analysis is performed with a slightly modified version of the dedicated tool from (Guidi et al. 2015). These modifications regard the quantification of foci and aim at providing a more accurate estimation of the quantity of fluorescence held inside each focus. The Gaussian fitting approach has been replaced by a template matching framework with a bank of 100 symmetric 2D Gaussian kernels with standard deviations ranging from 0.5 to 7 pixels. The position of each template is determined as the maximum of normalized cross correlation whereas the most suitable template for a single focus is selected by minimizing the sum of square differences between the Gaussian template and the data within a circular mask of radius twice the standard deviation. The foci are then defined as spherical objects with radii of two times the standard deviations of the matched templates. All foci that could not be fitted were considered as a cube of dimension 5×5×5. Variation of the box size did

not affect overall results. The foci intensity can thus be measured as the sum of the fluorescence signal inside its sphere. Furthermore, the proportion of intensity from a nucleus held inside each of its foci is also computed.

Sir3-GFP quantification

Quantification of Sir3-GFP signal was carried using microscopy. Briefly cells were segmented on the basis of trans signal using a modified version of CellX, and the intensity of 30 Z-stacks deconvolved imaged was summed. Deconvolution was carried using MetaMorph. For each cell the intensity/pixel was measured and normalized by the WT average.

Western blots

Protein extracts were prepared from 2 ODs of exponentially growing cultures (O.D ~1) using the post-alkaline extraction method (Kushnirov et al. 2000). For immunoblotting, we used custom-made rabbit polyclonal antibodies raised against full length Sir3 [1:10000 dilution] (Ruault et al. 2011).

FACS

Cell cycle profiles were obtained on a Accury FACS machine using CYTOX as DNA staining agent and analyzed using FlowJoX.

SGA screen

Query strain was obtained by transforming strain yAT-1949 with pGAL-SIR3-HPH, integrated within *TRP1*. The query strain was crossed with the collection of histone point mutants (Dai and Boeke 2012) following the selection steps described in (Tong et al. 2001), with selection media adapted to respective genotypes. Each cross was done in quadruplicate on 1536-format plates. Once double mutants were acquired, they were transferred to one of the following medium: double mutant selection medium (glucose), double mutant selection medium (glucose) + 5 mM NAM, double mutant selection medium (galactose) or double mutant selection medium (galactose) + 5 mM NAM. All strains were grown at 30^{o}C and imaged after 2 days. Image analysis and scoring were done with SGAtools (Wagih et al. 2013), where mutants growing on glucose media served as controls. Only significant changes were considered (p-val< 0.001) and a last significance threshold was chosen to only keep mutants which score's absolute value was > 0.2.

Dilution Assays

Cells were grown overnight in YPD 5 mM NAM before dilution. 5-fold serial dilutions are shown. Plates were grown for 2-3 days at 30°C .

Pellet preparation for ChIP

A total of 20 O.D equivalent of exponentially growing cells were fixed in 20 mL with 0.9 % formaldehyde for 15 min at 30°C, quenched with 0.125 M glycine and washed twice in cold TBS 1× pH 7.6. Pellets were suspended in 1mL TBS 1×, centrifuged and frozen in liquid nitrogen for -80°C storage. For NAM release experiments, Cells were grown overnight in YPD 5 mM NAM before dilution at 0.2 OD in YPD and allowed to grow for 8 hours (O.D ~1.5).

Chromatin immunoprecipitation

All following steps were done at 4°C unless indicated. Pellets were re-suspended in 500 µL of lysis buffer (0.01% SDS, 1.1% Triton X-100, 1.2 mM EDTA pH 8, 16.7 mM Tris pH8, 167 mM NaCl, 0.5 % BSA, 0.02 $g.L^{-1}$ tRNA and 2.5 µL of protease inhibitor from SIGMA P1860) and mechanically lysed by three cycles of 30s, intensity 6ms-1 with 500 µm zirconium/silica beads (Biospec Products) using a Fastprep instrument (MP Biomedicals). Each bead beating cycle was followed by 5 min incubation on ice. The chromatin was fragmented to a mean size of 500 bp by sonication in the Bioruptor XL (Diagenode) for 14 min at high power with 30 s on / 30 s off and centrifuged 5 min at 13 000 rpm. 10 µL were kept to be used as Input DNA. Cleared lysate was incubated overnight with 1 µL of polyclonal antibody anti-Sir3 (Ruault et al. 2011). 50 µL of magnetic beads protein A (NEB) were added to the mixture and incubated for 4h at 4°C. Magnetic beads were washed sequentially with lysis buffer, twice with RIPA buffer (0.1% SDS, 10 mM Tris pH7.6, 1 mM EDTA pH8, 0,1% sodium deoxycholate and 1% Triton X-100), twice with RIPA buffer supplemented with 300 mM NaCl, twice in LiCl buffer (250 mM LiCl, 0.5% NP40, 0.5 % sodium deoxycholate), with TE 0.2% Triton X-100 and with TE. Input were diluted 10× with elution buffer (50 mM Tris, 10 mM EDTA pH8, 1%SDS) and beads were re-suspended in 100 µL elution buffer. A reversal cross-linking was performed by heating samples overnight at 65°C. Proteins were digested with proteinase K in presence of glycogen and the remaining DNA was purified on QIAquick PCR purification columns. Finally, samples were treated with RNase A 30 min at 37°C.

ChIP-chip preparation and hybridation

Samples used for ChIP-chip have all been analysed by qPCR prior to microarray hybridization. For microarray hybridization 4/5 of the immunoprecipitated DNA and of the DNA from the input were ethanol precipitated and re-suspended in 10µL of water (Gibco). Purified material was amplified, incorporating amino-allyl-dUTP using as described in (Guidi et al.

2015). The size of amplified fragments (~500 bp) was assessed by gel electrophoresis. For each sample 1.5 µg of amplified DNA was coupled either with Cy5 (immunoprecipitated sample) or Cy3 (input sample) and hybridized on 44k yeast whole genome tiling array (Agilent) as described in (Guidi et al. 2015).

Microarray data acquisition, analysis and visualization

Microarray was imaged using a Agilent DNA microarray scanner and quantified using GenePix Pro6.1 as described in (Guidi et al. 2015).

Genome wide data analysis

Unless mentioned otherwise, data analysis was carried using R (R Core Team 2016). All datasets were lifted over to SacCer3 when required. Histone marks data were obtained from (Weiner et al. 2015). Sir3 binding in H3 tail mutants from (Sperling and Grunstein 2009), nucleosome turnover from (Dion et al. 2007). Transcriptome data were downloaded from the website supporting the publication (Kemmeren et al. 2014). Subtelomere definition was obtained from (Yue et al. 2017). Z-scores were computed using the R scale function. Criterion for the clustering of subtelomeres shown in Fig 1 were the following: First, the spreading end point was computed as the most subtelomeric probes with Sir3 binding Z-score >1 flanked by more than 5 probes with Z-score < 1. We then applied the following criterions: “Fragile” subtelomeres: d(TEF-ADH)<2 kb<d(ADH-WT) ; “Unextendable”: d(TEF-ADH), d(ADH-WT) <2 kb ; “Robust”: d(ADH-WT) <2 kb<d(TEF-ADH) ; “Progressive”: d(TEF-ADH), d(ADH-WT) >2 kb. Of note, 2 subtelomeres (*VIIR*, *XVIR*) which classification was too sensitive to a given threshold were manually curated. Euchromatic binding sites shown as supplemental table 1 were computed as sites away from ESDs (or present at more than 50 kb from a telomere when ESD are not defined) at which at least two neighbouring probes are bound (z-score >0.5) by Sir3 upon overexpression of *SIR3* (computed the signal obtained from the W303 strain yAT1254).

Downsampling of (Sperling and Grunstein 2009), (Mitsumori et al. 2016) and (Weiner et al. 2015) data to the 44k microarray probes for Fig 4B and 5A was done using R, visual inspection of the data confirmed that downsampling was carried without errors. In details, all signal located in between the mi-distance to the previous and the next probe were average and allocated to the central probe. Average telomeric profiles were done by computing the mean of the signal over 10 kb windows separated by 10 bp. The limits of Extended silent domains were computed as the first probes possessing 5 neighboring probes

that have Z-score inferior to 1, starting from the telomere. Fitting of Sir3 binding data was done using MATLAB fitting toolbox using Bisquare robustess option. The function used is f(x)=K/(1+exp(-r(-x+t0)))+1, with the following fitting parameters for K,r, and t0: lower bounds: [10 0.0001 1000], Starting point: [10 0.0001 1000], upper bounds: [200 0.01 40000]. Area under the curve was exactly computed on the fitted signal of Sir3 binding in strains overexpressing *SIR2* and *SIR3*, 10 kb before the end of silent domains and 5 kb after.

Mutants showing localized effects were identified with using the hypergeometric distribution, function phyper with Bonferroni correction for multiple testing (n=703 being the number of mutants studied showing significant transcription changes).

Linear model fitting of histone mark transition zones: For this plot subtelomeres differing between W303 and BY background were excluded (n=3, *TELIR*, *TELVIIL*, *TELXIVR*). For each viewpoints all subtelomeres in which the viewpoint is defined were considered. First, the length on which fitting was applied was optimized as the length giving the highest R-squared around ESDs. Window size ranging from 1 to 5 kb (100 bp step) were tried for each histone mark probed. Fitting of data on windows of defined size 20 kb around viewpoints with 50 bp steps was carried with the R lm() function.

RNA-seq

Total RNA from a 25mL culture of exponentially growing yeasts were extracted using phenol-chloroform. Banks were constructed using the kit SOLiD Total RNA-seq, with minor modifications: RNA are Zinc fragmented and fragments with size ranging from 100 to 200 nt selected by gel purification. After reverse transcription, only fragment of size > 150nt are kept. Paired end (50 + 35) sequencing was done by the Institut Curie plateform. Differential expression was called using edgeR (Robinson et al. 2010), with a false discovery rate inferior to 0.1.

Data access

ChIP-chip and RNA-seq data from this study have been submitted to the Gene Expression Omnibus (GEO; https://www.ncbi.nlm.nih.gov/geo/) under the accession numbers GSE106499, and GSE104391, respectively.

Acknowledgments

We thank T. Rio Frio, S. Baulande and P. Legoix-Né (NGS platform, Institut Curie), A. Lermine (bioinformatics platform, Institut Curie), P.Lebaccon (PICT@Pasteur microscopy platform) for support. We warmly thank Jacob Swadling and Alexander Esin for helping out with the language. We also thank Camille Gautier for help with multiple mapping reads analysis and Marta Kwapisz for RNA-seq library preparation. We thank Valérie Borde for help with microarray experiments, David Sitbon, Valérie Borde and Arnaud De Muyt for fruitful discussions, David Sitbon and Ann Ehrenhofer-Murray for critical reading of the manuscript. This work has benefited from the facilities and expertise of the NGS platform of Institut Curie (supported by the Agence Nationale de la Recherche [ANR-10-EQPX-03, ANR10-INBS-09-08] and the Canceropôle Ile-de-France). A. Morillon's lab is supported by the Agence Nationale de la Recherche (DNA-life) and the European Research Council (EpincRNA starting grant, DARK consolidator grant). A. Taddei's lab is supported by funding from the Labex DEEP (ANR-11-LABX-0044_DEEP and ANR-10-IDEX-0001-02 PSL), from the ANR DNA-Life (ANR-15-CE12-0007) and FRM grant DEP20131128535. AH was supported by fellowships from the ENS PhD program and the FRM (FDT20160435654).

Disclosure Declaration

None of the authors have any competing interests

References

Altaf M, Utley RT, Lacoste N, Tan S, Briggs SD, Cote J. 2007. Interplay of chromatin modifiers on a short basic patch of histone H4 tail defines the boundary of telomeric heterochromatin. *Mol Cell* **28**: 1002–1014.

Aparicio OM, Billington BL, Gottschling DE. 1991. Modifiers of position effect are shared between telomeric and silent mating-type loci in S. cerevisiae. *Cell* **66**: 1279–1287.

Armache K-J, Garlick JD, Canzio D, Narlikar GJ, Kingston RE. 2011. Structural Basis of Silencing: Sir3 BAH Domain in Complex with a Nucleosome at 3.0 A Resolution. *Science (80-)* **334**: 977–982.

Batté A, Brocas C, Bordelet H, Hocher A, Ruault M, Adjiri A, Taddei A, Dubrana K. 2017. Recombination at subtelomeres is regulated by physical distance, double-strand break resection and chromatin status. *EMBO J* e201796631.

Behrouzi R, Lu C, Currie M, Jih G, Iglesias N, Moazed D. 2016. Heterochromatin assembly by interrupted Sir3 bridges across neighboring nucleosomes. *Elife* **5**.

Bi X. 2002. Domains of gene silencing near the left end of chromosome III in Saccharomyces cerevisiae. *Genetics* **160**: 1401–1407.

Bi X, Braunstein M, Shei GJ, Broach JR. 1999. The yeast HML I silencer defines a heterochromatin domain boundary by directional establishment of silencing. *Proc Natl*

Acad Sci U S A **96**: 11934–11939.
Bitterman KJ, Anderson RM, Cohen HY, Latorre-Esteves M, Sinclair DA. 2002. Inhibition of silencing and accelerated aging by nicotinamide, a putative negative regulator of yeast Sir2 and human SIRT1. *J Biol Chem* **277**: 45099–45107.
Carmen AA, Milne L, Grunstein M. 2002. Acetylation of the yeast histone H4 N terminus regulates its binding to heterochromatin protein SIR3. *J Biol Chem* **277**: 4778–4781.
Choe W, Budd M, Imamura O, Hoopes L, Campbell JL. 2002. Dynamic localization of an Okazaki fragment processing protein suggests a novel role in telomere replication. *Mol Cell Biol* **22**: 4202–4217..
Dai J, Boeke JD. 2012. Strain construction and screening methods for a yeast histone H3/H4 mutant library. *Methods Mol Biol* **833**: 1–14.
Deutschbauer AM, Jaramillo DF, Proctor M, Kumm J, Hillenmeyer ME, Davis RW, Nislow C, Giaever G. 2005. Mechanisms of haploinsufficiency revealed by genome-wide profiling in yeast. *Genetics* **169**: 1915–1925.
Dion MF, Kaplan T, Kim M, Buratowski S, Friedman N, Rando OJ. 2007. Dynamics of replication-independent histone turnover in budding yeast. *Science* **315**: 1405–8.
Donze D, Adams CR, Rine J, Kamakaka RT. 1999. The boundaries of the silenced HMR domain in Saccharomyces cerevisiae. *Genes Dev* **13**: 698–708.
Donze D, Kamakaka RT. 2002. Braking the silence: How heterochromatic gene repression is stopped in its tracks. *BioEssays* **24**: 344–349.
Donze D, Kamakaka RT. 2001. RNA polymerase III and RNA polymerase II promoter complexes are heterochromatin barriers in Saccharomyces cerevisiae. *EMBO J* **20**: 520–531.
Ellahi A, Thurtle DM, Rine J. 2015. The chromatin and transcriptional landscape of native saccharomyces cerevisiae telomeres and subtelomeric domains. *Genetics* **200**: 505–521.
Emil H. 1928. Das Heterochromatin der Moose. *Jahrbücher für Wissenschaftliche Bot* **69**: 762–818.
Gartenberg MR, Smith JS. 2016. The nuts and bolts of transcriptionally silent chromatin in Saccharomyces cerevisiae. *Genetics* **203**: 1563–1599.
Gotta M, Laroche T, Formenton A, Maillet L, Scherthan H, Gasser SM. 1996. The clustering of telomeres and colocalization with Rap1, Sir3, and Sir4 proteins in wild-type Saccharomyces cerevisiae. *J Cell Biol* **134**: 1349–1363.
Grewal SIS, Jia S. 2007. Heterochromatin revisited. *Nat Rev Genet* **8**: 35–46.
Grunstein M. 1997. Molecular model for telomeric heterochromatin in yeast. *Curr Opin Cell Biol* **9**: 383–387.
Grunstein M, Gasser SM. 2013. Epigenetics in Saccharomyces cerevisiae. *Cold Spring Harb Perspect Biol* **5**.
Guidi M, Ruault M, Marbouty M, Loïodice I, Cournac A, Billaudeau C, Hocher A, Mozziconacci J, Koszul R, Taddei A. 2015. Spatial reorganization of telomeres in long-lived quiescent cells. *Genome Biol*.
Guillemette B, Bataille AR, Gévry N, Adam M, Blanchette M, Robert F, Gaudreau L. 2005. Variant histone H2A.z is globally localized to the promoters of inactive yeast genes and regulates nucleosome positioning. *PLoS Biol* **3**: 1–11.
Guintini L, Tremblay M, Toussaint M, D'Amours A, Wellinger RE, Wellinger RJ, Conconi A. 2017. Repair of UV-induced DNA lesions in natural Saccharomyces cerevisiae telomeres is moderated by Sir2 and Sir3, and inhibited by yKu-Sir4 interaction. *Nucleic Acids Res* **45**: 4577–4589.

Harbison CT, Gordon DB, Lee TI, Rinaldi NJ, Macisaac KD, Danford TW, Hannett NM, Tagne J-B, Reynolds DB, Yoo J, et al. 2004. Transcriptional regulatory code of a eukaryotic genome. *Nature* **431**: 99–104.

Hecht A, Strahl-Bolsinger S, Grunstein M. 1996. Spreading of transcriptional repressor SIR3 from telomeric heterochromatin. *Nature* **383**: 92–96.

Hoppe GJ, Tanny JC, Rudner AD, Gerber SA, Danaie S, Gygi SP, Moazed D. 2002. Steps in assembly of silent chromatin in yeast: Sir3-independent binding of a Sir2/Sir4 complex to silencers and role for Sir2-dependent deacetylation. *Mol Cell Biol* **12**: 4167–4180.

Kasinathan S, Orsi GA, Zentner GE, Ahmad K, Henikoff S. 2014. High-resolution mapping of transcription factor binding sites on native chromatin. *Nat Methods* **11**: 203–209.

Katan-Khaykovich Y, Struhl K. 2005. Heterochromatin formation involves changes in histone modifications over multiple cell generations. *EMBO J* **24**: 2138–2149.

Kemmeren P, Sameith K, Van De Pasch LAL, Benschop JJ, Lenstra TL, Margaritis T, O'Duibhir E, Apweiler E, Van Wageningen S, Ko CW, et al. 2014. Large-scale genetic perturbations reveal regulatory networks and an abundance of gene-specific repressors. *Cell* **157**: 740–752.

Kitada T, Kuryan BG, Tran NN, Song C, Xue Y, Carey M, Grunstein M. 2012. Mechanism for epigenetic variegation of gene expression at yeast telomeric heterochromatin. *Genes Dev* **26**: 2443–2455.

Kitada T, Schleker T, Sperling AS, Xie W, Gasser SM, Grunstein M. 2011. ??H2A is a component of yeast heterochromatin required for telomere elongation. *Cell Cycle* **10**: 293–300.

Kristjuhan A, Wittschieben BO, Walker J, Roberts D, Cairns BR, Svejstrup JQ. 2003. Spreading of Sir3 protein in cells with severe histone H3 hypoacetylation. *Proc Natl Acad Sci U S A* **100**: 7551–7556.

Lenstra TL, Benschop JJ, Kim T, Schulze JM, Brabers NACH, Margaritis T, van de Pasch LAL, van Heesch SAAC, Brok MO, Groot Koerkamp MJA, et al. 2011. The Specificity and Topology of Chromatin Interaction Pathways in Yeast. *Mol Cell* **42**: 536–549.

Lieb JD, Liu X, Botstein D, Brown PO. 2001. Promoter-specific binding of Rap1 revealed by genome-wide maps of protein-DNA association. *Nat Genet* **28**: 327–334.

Louis E, Becker M. 2014. Subtelomeres. *Springer,* ISBN 978-3-642-41566-1

Marchfelder U, Rateitschak K, Ehrenhofer-Murray AE. 2003. SIR-dependent repression of non-telomeric genes in Saccharomyces cerevisiae? *Yeast* **20**: 797–801.

Martino F, Kueng S, Robinson P, Tsai-Pflugfelder M, van Leeuwen F, Ziegler M, Cubizolles F, Cockell MM, Rhodes D, Gasser SM. 2009. Reconstitution of yeast silent chromatin: multiple contact sites and O-AADPR binding load SIR complexes onto nucleosomes in vitro. *Mol Cell* **33**: 323–334.

Martins-Taylor K, Sharma U, Rozario T, Holmes SG. 2011. H2A.Z (Htz1) controls the cell-cycle-dependent establishment of transcriptional silencing at Saccharomyces cerevisiae telomeres. *Genetics* **187**: 89–104.

Matsuda A, Chikashige Y, Ding D-Q, Ohtsuki C, Mori C, Asakawa H, Kimura H, Haraguchi T, Hiraoka Y. 2015. Highly condensed chromatins are formed adjacent to subtelomeric and decondensed silent chromatin in fission yeast. *Nat Commun* **6**: 7753.

Meneghini MD, Wu M, Madhani HD. 2003. Conserved histone variant H2A.Z protects euchromatin from the ectopic spread of silent heterochromatin. *Cell* **112**: 725–36.

Millar CB, Grunstein M. 2006. Genome-wide patterns of histone modifications in yeast. *Nat Rev Mol Cell Biol* **7**: 657–66.

Mitsumori R, Ohashi T, Kugou K, Ichino A, Taniguchi K, Ohta K, Uchida H, Oki M. 2016. Analysis of novel Sir3 binding regions in Saccharomyces cerevisiae. *J Biochem* **160**: 11–17.

Moazed D, Kistler A, Axelrod A, Rine J, Johnson AD. 1997. Silent information regulator protein complexes in Saccharomyces cerevisiae: a SIR2/SIR4 complex and evidence for a regulatory domain in SIR4 that inhibits its interaction with SIR3. *Proc Natl Acad Sci U S A* **94**: 2186–91.

Ng HH, Feng Q, Wang H, Erdjument-Bromage H, Tempst P, Zhang Y, Struhl K. 2002. Lysine methylation within the globular domain of histone H3 by Dot1 is important for telomeric silencing and Sir protein association. *Genes Dev* **16**: 1518–1527.

Oki M, Valenzuela L, Chiba T, Ito T, Kamakaka RT. 2004. Barrier proteins remodel and modify chromatin to restrict silenced domains. *Mol Cell Biol* **24**: 1956–1967.

Osborne EA, Dudoit S, Rine J. 2009. The establishment of gene silencing at single-cell resolution. *Nat Genet* **41**: 800–806.

Park D, Lee Y, Bhupindersingh G, Iyer VR. 2013. Widespread misinterpretable ChIP-seq bias in yeast. *PLoS One* **8**.

Pelechano V, Chávez S, Pérez-Ortín JE. 2010. A complete set of nascent transcription rates for yeast genes. *PLoS One* **5**.

Peng J, Zhou JQ. 2012. The tail-module of yeast Mediator complex is required for telomere heterochromatin maintenance. *Nucleic Acids Res* **40**: 581–593.

Preti M, Ribeyre C, Pascali C, Bosio MC, Cortelazzi B, Rougemont J, Guarnera E, Naef F, Shore D, Dieci G. 2010. The Telomere-Binding Protein Tbf1 Demarcates snoRNA Gene Promoters in Saccharomyces cerevisiae. *Mol Cell* **38**: 614–620.

Pryde FE, Louis EJ. 1999. Limitations of silencing at native yeast telomeres. *EMBO J* **18**: 2538–2550.

Radman-Livaja M, Ruben G, Weiner A, Friedman N, Kamakaka R, Rando OJ. 2011. Dynamics of Sir3 spreading in budding yeast: secondary recruitment sites and euchromatic localization. *EMBO J* **30**: 1012–1026.

R Core Team. 2016. R: a language and environment for statistical computing. R Foundation for Statistical Computing, Vienna, Austria. https://www.R-project.org/.

Renauld H, Aparicio OM, Zierath PD, Billington BL, Chhablani SK, Gottschling DE. 1993a. Silent domains are assembled continuously from the telomere and are defined by promoter distance and strength, and by SIR3 dosage. *Genes Dev* **7**: 1133–1145.

Renauld H, Aparicio OM, Zierath PD, Billington BL, Chhablani SK, Gottschling DE. 1993b. Silent domains are assembled continuously from the telomere and are defined by promoter distance and strength, and by SIR3 dosage. *Genes Dev* **7**: 1133–1145.

Rhee HS, Pugh BF. 2012. ChiP-exo method for identifying genomic location of DNA-binding proteins with near-single-nucleotide accuracy. *Curr Protoc Mol Biol*.

Richards EJ, Elgin SCR. 2002. Epigenetic codes for heterochromatin formation and silencing: Rounding up the usual suspects. *Cell* **108**: 489–500.

Rine J, Herskowitz I. 1987. Four genes responsible for a position effect on expression from HML and HMR in Saccharomyces cerevisiae. *Genetics* **116**: 9–22.

Robinson M, McCarthy D, Chen Y, Smyth GKG. 2010. edgeR: differential expression analysis of digital gene expression data. *R Man* 1–76.

Robyr D, Suka Y, Xenarios I, Kurdistani SK, Wang A, Suka N, Grunstein M. 2002. Microarray deacetylation maps determine genome-wide functions for yeast histone deacetylases. *Cell* **109**: 437–46.

Roy R, Meier B, McAinsh AD, Feldmann HM, Jackson SP. 2004. Separation-of-function mutants of yeast Ku80 reveal a Yku80p-Sir4p interaction involved in telomeric silencing. *J Biol Chem* **279**: 86–94.

Ruault M, De Meyer A, Loiodice I, Taddei A. 2011a. Clustering heterochromatin: Sir3 promotes telomere clustering independently of silencing in yeast. *J Cell Biol* **192**: 417–431.

Ruault M, De Meyer A, Loiodice I, Taddei A. 2011b. Clustering heterochromatin: Sir3 promotes telomere clustering independently of silencing in yeast. *J Cell Biol* **192**: 417–431.

Rudner AD, Hall BE, Ellenberger T, Moazed D. 2005. A nonhistone protein-protein interaction required for assembly of the SIR complex and silent chromatin. *Mol Cell Biol* **25**: 4514–4528.

Rusche LN, Kirchmaier AL, Rine J. 2003. The establishment, inheritance, and function of silenced chromatin in Saccharomyces cerevisiae. *Annu Rev Biochem* **72**: 481–516.

Schulze JM, Jackson J, Nakanishi S, Gardner JM, Hentrich T, Haug J, Johnston M, Jaspersen SL, Kobor MS, Shilatifard A. 2009. Linking Cell Cycle to Histone Modifications: SBF and H2B Monoubiquitination Machinery and Cell-Cycle Regulation of H3K79 Dimethylation. *Mol Cell* **35**: 626–641.

Shampay J, Szostak JW, Blackburn EH. 1984. DNA sequences of telomeres maintained in yeast. *Nature* **310**: 154–157.

Sperling AS, Grunstein M. 2009. Histone H3 N-terminus regulates higher order structure of yeast heterochromatin. *Proc Natl Acad Sci U S A* **106**: 13153–13159.

Strahl-Bolsinger S, Hecht A, Luo K, Grunstein M. 1997. SIR2 and SIR4 interactions differ in core and extended telomeric heterochromatin in yeast. *Genes Dev* **11**: 83–93.

Stulemeijer IJE, De Vos D, van Harten K, Joshi OK, Blomberg O, van Welsem T, Terweij M, Vlaming H, de Graaf EL, Altelaar a. FM, et al. 2015. Dot1 histone methyltransferases share a distributive mechanism but have highly diverged catalytic properties. *Sci Rep* **5**: 1–11.

Suka N, Luo K, Grunstein M. 2002. Sir2p and Sas2p opposingly regulate acetylation of yeast histone H4 lysine16 and spreading of heterochromatin. *Nat Genet* **32**: 378–83.

Szilard RK, Jacques PE, Laramee L, Cheng B, Galicia S, Bataille AR, Yeung M, Mendez M, Bergeron M, Robert F, et al. 2010. Systematic identification of fragile sites via genome-wide location analysis of gamma-H2AX. *Nat Struct Mol Biol* **17**: 299–305.

Talbert PB, Henikoff S. 2006. Spreading of silent chromatin: inaction at a distance. *Nat Rev Genet* **7**: 793–803.

Teytelman L, Thurtle DM, Rine J, van Oudenaarden A. 2013. Highly expressed loci are vulnerable to misleading ChIP localization of multiple unrelated proteins. *Proc Natl Acad Sci U S A* **110**: 18602–18607.

Tong AH, Evangelista M, Parsons AB, Xu H, Bader GD, Pagé N, Robinson M, Raghibizadeh S, Hogue CW, Bussey H, et al. 2001. Systematic genetic analysis with ordered arrays of yeast deletion mutants. *Science* **294**: 2364–8.

Tsukamoto Y, Kato J-I, Ikeda H. 1997. Silencing factors participate in DNA repair and recombination in Saccharomyces cerevisiae. *Nature* **388**: 900–903.

Van De Vosse DW, Wan Y, Lapetina DL, Chen WM, Chiang JH, Aitchison JD, Wozniak RW. 2013. A role for the nucleoporin Nup170p in chromatin structure and gene silencing. *Cell* **152**: 969–983.

Wang F, Li G, Altaf M, Lu C, Currie MA, Johnson A, Moazed D. 2013. Heterochromatin protein

Sir3 induces contacts between the amino terminus of histone H4 and nucleosomal DNA. *Proc Natl Acad Sci U S A* **110**: 8495–8500.

Wang J, Jia ST, Jia S. 2016. New Insights into the Regulation of Heterochromatin. *Trends Genet* **32**: 284–294.

Weiner A, Hsieh TH, Appleboim A, Chen H V, Rahat A, Amit I, Rando OJ, Friedman N. 2015. High-Resolution Chromatin Dynamics during a Yeast Stress Response. *Mol Cell* **58**: 371–386.

Yu MC, Lamming DW, Eskin JA, Sinclair DA, Silver PA. 2006. The role of protein arginine methylation in the formation of silent chromatin. *Genes Dev* **20**: 3249–3254.

Yue J-X, Li J, Aigrain L, Hallin J, Persson K, Oliver K, Bergström A, Coupland P, Warringer J, Lagomarsino MC, et al. 2017. Contrasting evolutionary genome dynamics between domesticated and wild yeasts. *Nat Genet* **49**: 913–924.

Figure legends

Figure 1: Increasing Sir3 dosage leads to telomere clustering and SIR spreading saturation. (A) Quantification of Sir3 levels by integration of Sir3-GFP signal in strains expressing *SIR3-GFP* under different promoters as indicated. (B) ChIP-chip against Sir3 was carried in strains expressing *SIR3* under different promoters as indicated. Moving average of Sir3 binding (block = 1000 bp, window = 10 bp) at telomeres (with the exception of *TELIIIL* and *TELIIIR* that contain *HM* loci) as a function of distance from the *ARS* consensus sequence (ACS) within the last telomeric element. Enrichment is shown as the standardized IP over Input (See mat and meth). (C) Rap1-GFP foci grouping in strain differing for Sir3 levels. Cells were grown in YPD overnight, diluted to OD600 nm= 0.2 and imaged at OD600 nm= 1. (D) Quantification of Rap1-GFP foci distribution in images from C. (E) Left: Distribution of Rap1-GFP signal attributed to the brightest foci in each nucleus; Right: Distribution of the relative amount of Rap1 measured within foci relative to total nuclear Rap1 signal. (F) Stereotypical examples of Sir3 binding in function of Sir3 dosage. Enrichment corresponds to standardized Sir3 binding (z-score). The number of subtelomeres within each group is shown into bracket.

Figure 2: Sir3 extended domains are silenced and restricted to subtelomeres. (A) Representative Rap1-GFP images of exponentially growing strains with different Sir3 amount or expressing the *SIR3-A2Q* point mutant allele. (B) Chromosome wide binding of Sir3 in the same strains as in A and blow-up on subtelomere *VIR*. Enrichment is shown as the standardized IP over Input and scale is thresholded at 15 for visualization purposes. (C) Total RNAseq read density and corresponding transcriptional fold change along subtelomere VIR in indicated exponentially growing (OD600 nm~1) strains. (D) Sir3 binding and corresponding transcription changes of subtelomeric genes (Distance from chromosome end <50 kb) upon overexpression of *SIR3*. Genes showing infinite fold change values were excluded from this plot. Color code indicates if a gene is annotated as within ESDs (see math and meth) and shade indicates significance (FDR<0.1) of the detected changes. Read density in *WT* cells is proportional to the disk area. Black line corresponds to linear fitting of the data, and corresponding R-squared value is shown. (E) Exemplification of the 7 subtelomeres at which a gene within the ESD shows larger transcript amount than the genes located at the end of the domain. (F) Read density of genes located before and after the end of extended silent domains compared to genome wide distribution, statistical test: Wilcoxon test, paired values.

Figure 3: **End of extended silent domains is defined locally and independently of transcriptional activity.** (A) Sir3 binding at native and truncated *TELVIIL*, x coordinates correspond the native telomere *TELVIIL*. (B) Sir3 binding at *TELVL* in *WT* and Sir3 overexpressing (*pGPD-SIR3*) strains. Transcription factor (TF) binding and DNase I hypersensitive sites along *TELVL* are shown.

Figure 4: ESDs encompass known domains of Sir3 extension. (A) Moving average of Sir3 binding (block = 1000 bp, window = 10) at the end of ESDs in the indicated conditions or mutants. (B) Genome browser visualization of Sir3 binding at subtelomere *IIR*, all data are shown as Z-score with a lower bound of -1 and an upper bound of 12.

Figure 5: Extension of silent domains predicts major subtelomeric chromatin transitions. (A) Pearson correlation matrix between Sir3 binding and histone marks, *SIR3 oe* corresponds

to yAT1254 and *SIR2* & *SIR3 oe* to yAT1668. Histone modification data from Weiner et al. 2015 for all marks except H3K79me2 (Schulze et al. 2009). (B) Genome browser visualization of Sir3 binding in *WT*, *pGPD-SIR2 pGPD-SIR3* strains, in G1 blocked cells, in H3Δ4-30 mutants and selected histone modifications (from Weiner et al. 2015) in *WT* strains at *TELVIR*. (C) Distribution of selected histone marks relative to H3 (data from Weiner et al. 2015) along wild type silenced domains and within the contiguous subtelomeric domains accessible to Sir3 upon overexpression. For comparison, the distributions of those marks within the 5 kb contiguous to the end of extended silent domains as well as within euchromatin (*i.e*. ESD excluded, n=49313) are shown.

Figure 6: H3K79 methylation is key to sustain viability upon Sir3 overexpression. (A) Moving average of Sir3 binding at telomeres (10 kb windows, 10 bp step). The top and bottom 10 telomeres with regards to Sir3 signal in strains overexpressing *SIR2* and *SIR3* were plotted separately. H3K79me3 data were obtained from Weiner et al. 2015. Blue lines indicate genome wide lower and higher quartiles for each mark. Red line corresponds to the local smoothing of histone modification data. (B) Dilution assay to probe viability of *dot1* mutants upon overexpression of *SIR3*. Cells were constantly grown in presence of 5 mM NAM prior to this assay. Cells were grown overnight, and 0.5 OD of cells were plated in 5× serial dilutions on YPD or YPD 5 mM NAM. (C) Growth score of selected histone point mutants on galactose plates (Sir3 inducing conditions) with or without NAM compared to glucose plates (Sir3 dosage is *WT*). (D) Genome browser visualization of Sir3 binding in *pGPD-SIR3* and *dot1Δ pGPD-SIR3* strains 8 hours after being released from 5 mM NAM. *KRR1* and *CDC39*, labelled in red, are essential genes. H3K79 methylation enrichment were obtained from Weiner et al. 2015 for H3K79me and H3K79me3 and from Schulze et al. 2009 for H3K79me2 (Mat score is shown). (E) Moving average of Sir3 binding (block = 1000 bp, window = 10 bp) at the end of ESDs in *pGPD-SIR3* and *dot1Δ pGPD-SIR3* strains 8 hours after being released from 5 mM NAM. (F) Dot plot showing Sir3 enrichment in the indicated strains and condition against the enrichment for each methylation level of H3K79. H3K79 methylation data were obtained from the same source as in E and averaged at each ChIP-chip probe.

Figure 7: Extension of silent domains reveals new aspects of subtelomeric structuration. (A) Localized effects of mutations affecting subtelomeric transcription. The different subtelomeric subdomains are defined according to Sir3 binding. The number of genes within each domain is into brackets. Mutant names are positioned according to the domain(s) within which the proportion of genes up or down-regulated (log(FC)>1 or < -1) is significantly elevated (Hyper-geometric law, with Bonferonni correction n=703). (B) Distribution of H3K79me3 and H2AS129ph (obtained from Weiner et al. 2015) relative to different subtelomeric viewpoints. Blue lines indicate genome wide lower and higher quartiles for each mark. Red line corresponds to the LOESS smoothing of histone modification data. (C) Quantification of H3K79me3 transition in function of different genomic viewpoints. Shown are the results of a linear model fitting of the histone mark enrichment data (residuals standard deviation, slopes, R^2 and p-values) over 2.35 kb windows every 50 bp. (D) Model depicting how extending silent domains enables to uncover consistent subtelomeric domains delimited by chromatin mark transitions.

Hocher_Fig1

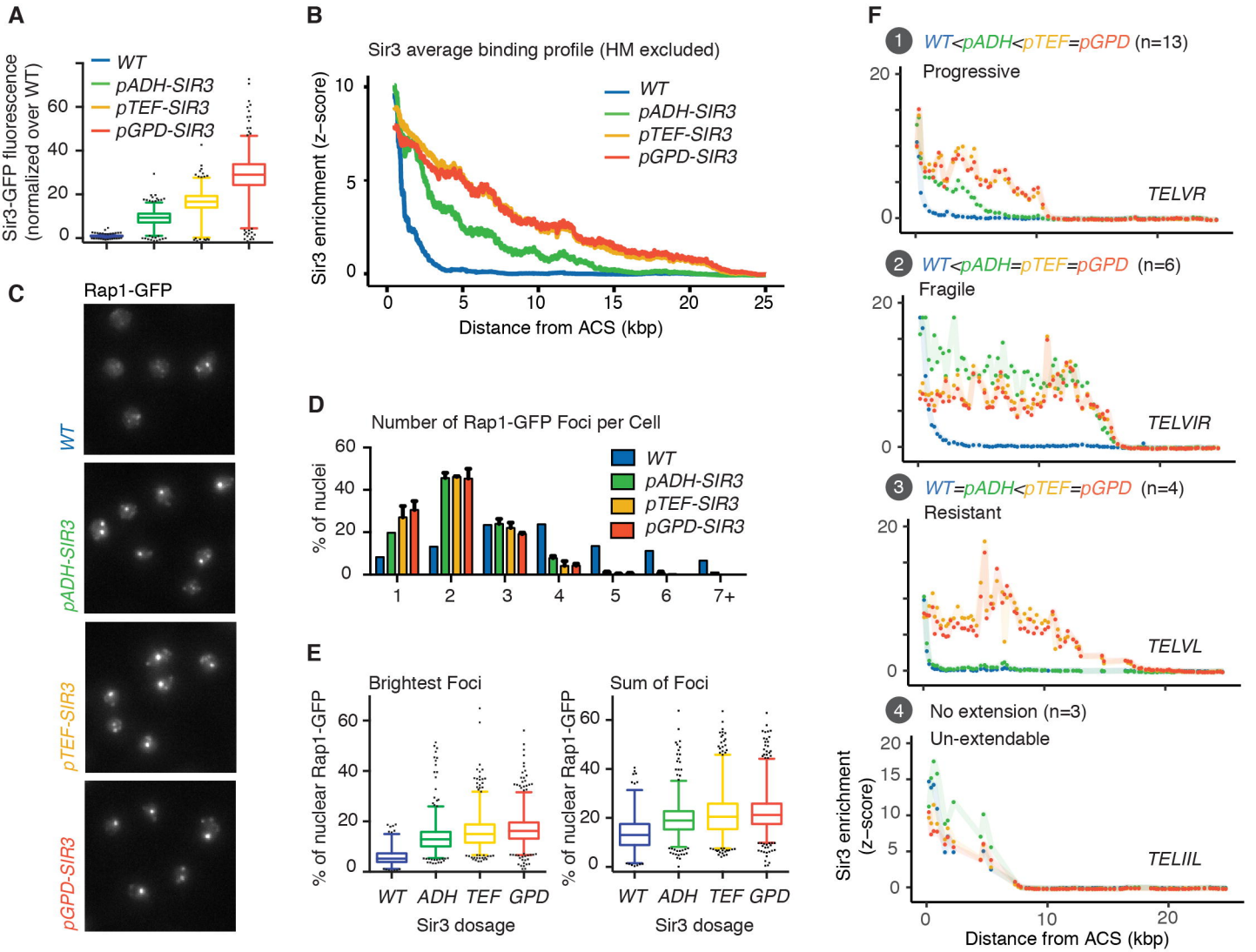
A
Sir3-GFP fluorescence (normalized over WT)
WT
pADH-SIR3
pTEF-SIR3
pGPD-SIR3
B
Sir3 average binding profile (HM excluded)
Sir3 enrichment (z-score)
Distance from ACS (kbp)
C
Rap1-GFP
WT
pADH-SIR3
pTEF-SIR3
pGPD-SIR3
D
Number of Rap1-GFP Foci per Cell
% of nuclei
E
Brightest Foci
Sum of Foci
% of nuclear Rap1-GFP
WT ADH TEF GPD
Sir3 dosage
F
1 WT<pADH<pTEF=pGPD (n=13)
Progressive
TELVR
2 WT<pADH=pTEF=pGPD (n=6)
Fragile
TELVIR
3 WT=pADH<pTEF=pGPD (n=4)
Resistant
TELVL
4 No extension (n=3)
Un-extendable
TELIIL
Sir3 enrichment (z-score)
Distance from ACS (kbp)

Hocher_Fig2

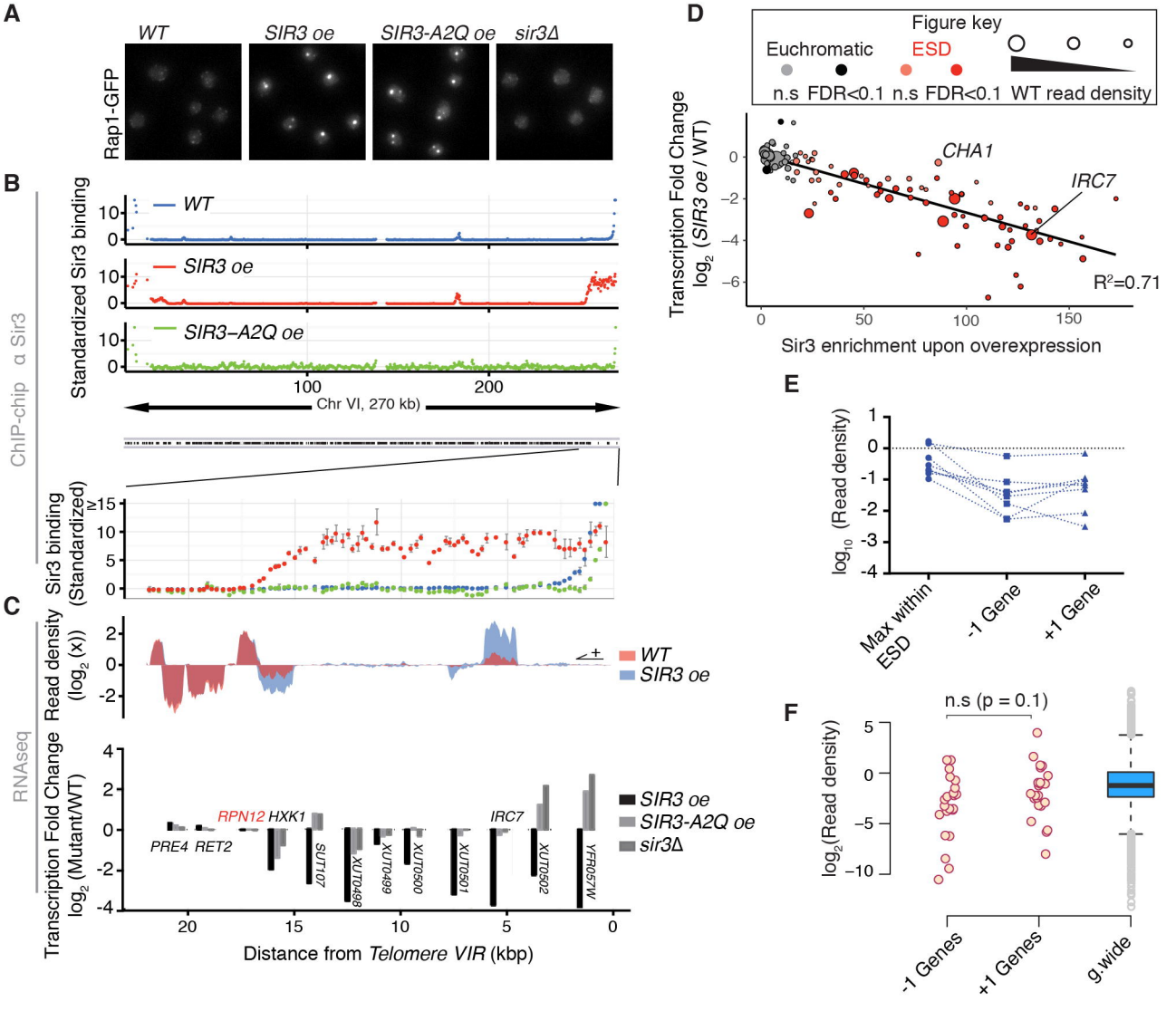
A
WT
SIR3 oe
SIR3-A2Q oe
sir3Δ
Rap1-GFP
B
ChIP-chip α Sir3
Standardized Sir3 binding
WT
SIR3 oe
SIR3–A2Q oe
Chr VI, 270 kb)
Sir3 binding (Standardized)
C
RNAseq
Read density (log2 (x))
WT
SIR3 oe
Transcription Fold Change log2 (Mutant/WT)
SIR3 oe
SIR3-A2Q oe
sir3Δ
RPN12
HXK1
IRC7
PRE4
RET2
SUT107
XUT0498
XUT0499
XUT0500
XUT0501
XUT0502
YFR057W
Distance from Telomere VIR (kbp)
D
Figure key
Euchromatic
ESD
n.s FDR<0.1 n.s FDR<0.1 WT read density
Transcription Fold Change log2 (SIR3 oe / WT)
CHA1
IRC7
R²=0.71
Sir3 enrichment upon overexpression
E
log10 (Read density)
Max within ESD
-1 Gene
+1 Gene
F
log2 (Read density)
n.s (p = 0.1)
-1 Genes
+1 Genes
g.wide

Hocher_Fig3

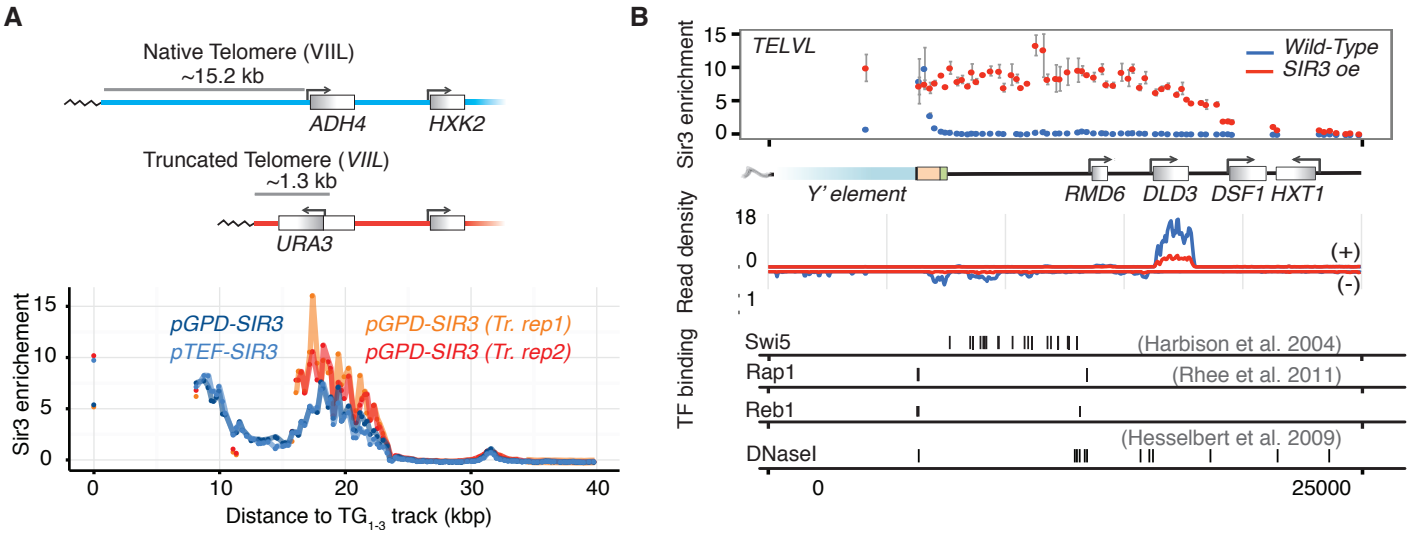
A
Native Telomere (VIIL)
~15.2 kb
ADH4
HXK2
Truncated Telomere (VIIL)
~1.3 kb
URA3
Sir3 enrichement
pGPD-SIR3
pTEF-SIR3
pGPD-SIR3 (Tr. rep1)
pGPD-SIR3 (Tr. rep2)
Distance to TG1-3 track (kbp)
B
Sir3 enrichment
TELVL
Wild-Type
SIR3 oe
Y' element
RMD6
DLD3
DSF1
HXT1
Read density
(+)
(-)
TF binding
Swi5
(Harbison et al. 2004)
Rap1
(Rhee et al. 2011)
Reb1
(Hesselbert et al. 2009)
DNaseI
25000

Hocher_Fig4

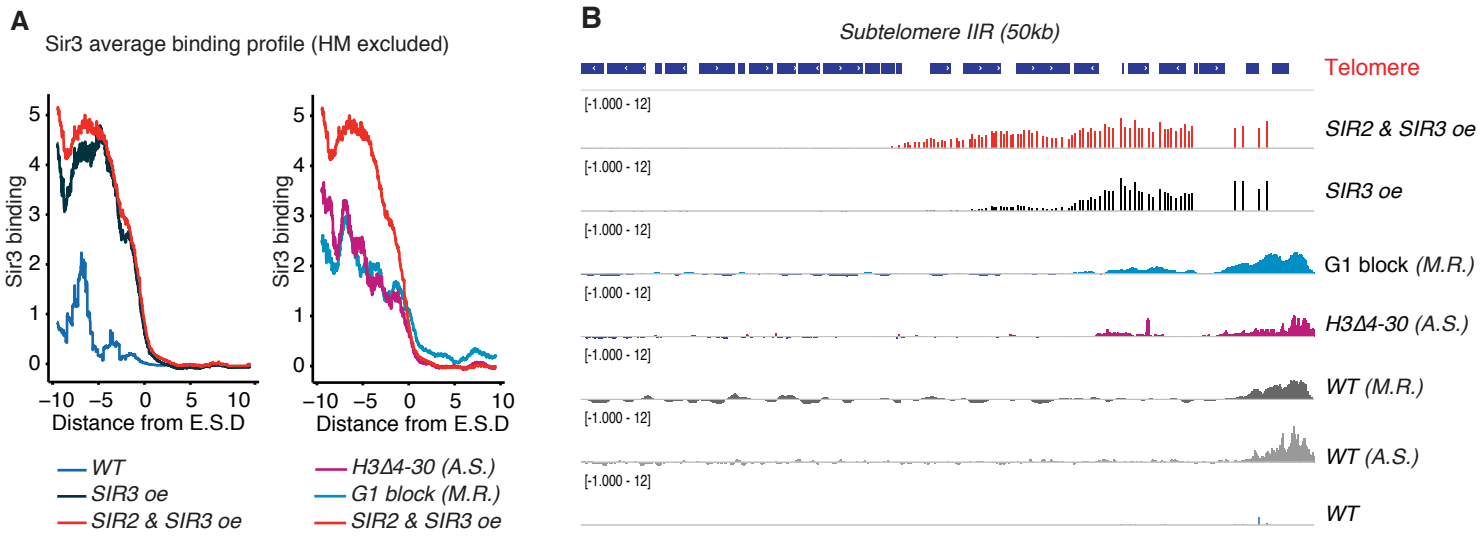
A
Sir3 average binding profile (HM excluded)
Sir3 binding
Distance from E.S.D
WT
SIR3 oe
SIR2 & SIR3 oe
H3Δ4-30 (A.S.)
G1 block (M.R.)
SIR2 & SIR3 oe
B
Subtelomere IIR (50kb)
Telomere
[-1.000 - 12]
SIR2 & SIR3 oe
SIR3 oe
G1 block (M.R.)
H3Δ4-30 (A.S.)
WT (M.R.)
WT (A.S.)
WT

Hocher_Fig5

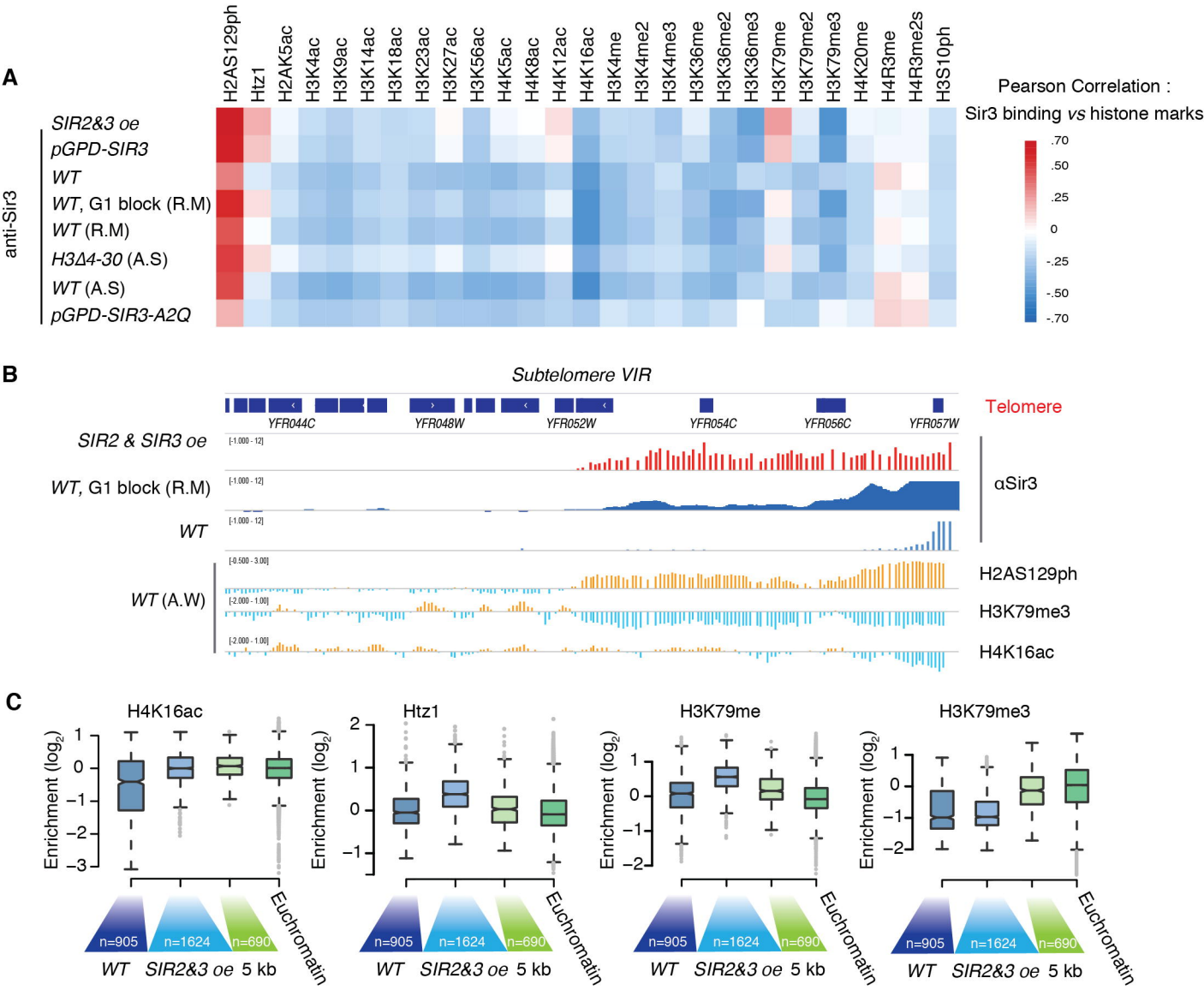
A
H2AS129ph
Htz1
H2AK5ac
H3K4ac
H3K9ac
H3K14ac
H3K18ac
H3K23ac
H3K27ac
H3K56ac
H4K5ac
H4K8ac
H4K12ac
H4K16ac
H3K4me
H3K4me2
H3K4me3
H3K36me
H3K36me2
H3K36me3
H3K79me
H3K79me2
H3K79me3
H4K20me
H4R3me
H4R3me2s
H3S10ph
anti-Sir3
SIR2&3 oe
pGPD-SIR3
WT
WT, G1 block (R.M)
WT (R.M)
H3Δ4-30 (A.S)
WT (A.S)
pGPD-SIR3-A2Q
Pearson Correlation :
Sir3 binding vs histone marks
.70
.50
.25
0
-.25
-.50
-.70
B
Subtelomere VIR
Telomere
YFR044C
YFR048W
YFR052W
YFR054C
YFR056C
YFR057W
SIR2 & SIR3 oe
WT, G1 block (R.M)
WT
WT (A.W)
αSir3
H2AS129ph
H3K79me3
H4K16ac
C
H4K16ac
Htz1
H3K79me
H3K79me3
Enrichment (log2)
n=905
n=1624
n=690
Euchromatin
WT
SIR2&3 oe
5 kb

HOCHER_Fig6

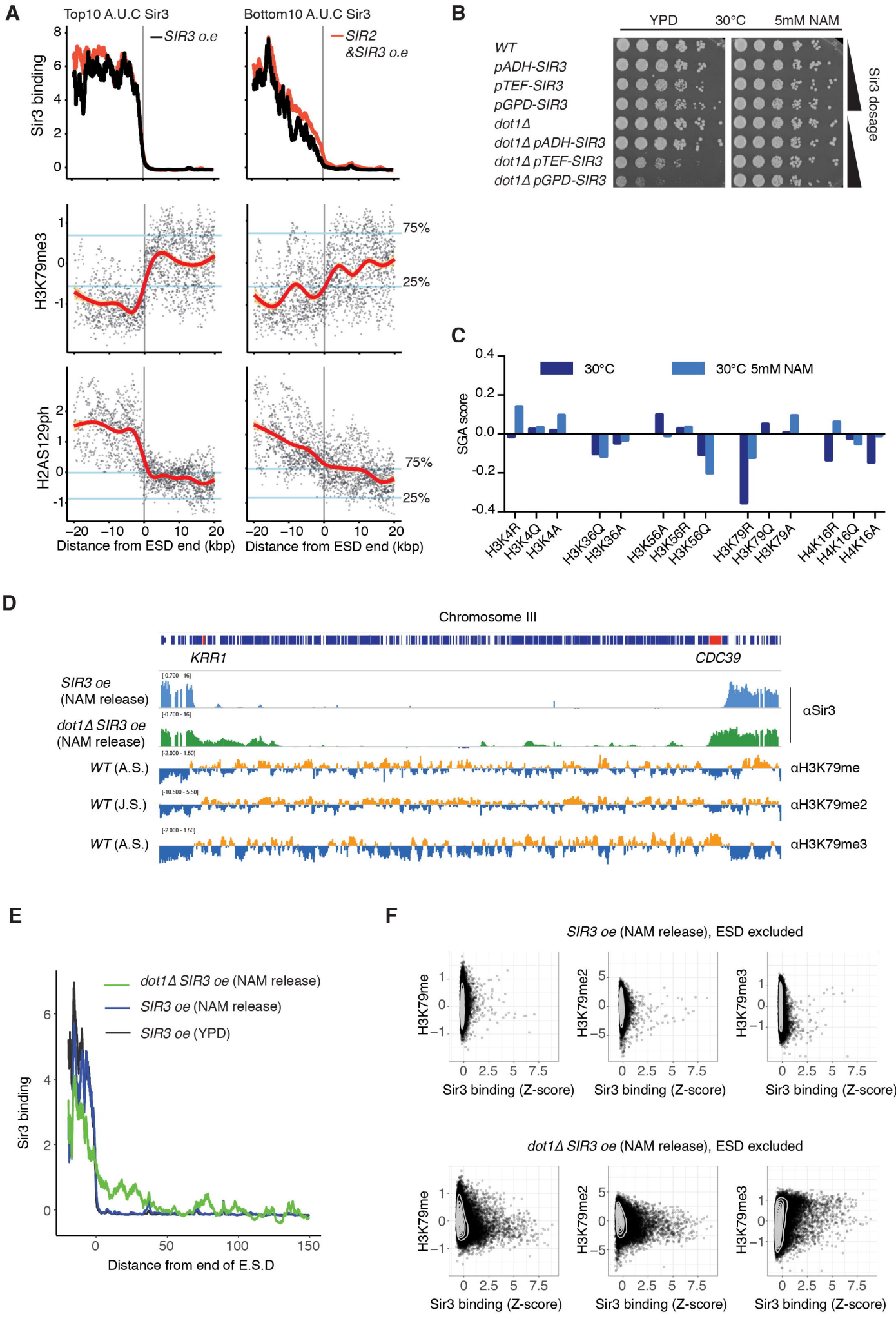
A
Top10 A.U.C Sir3
Bottom10 A.U.C Sir3
SIR3 o.e
SIR2 &SIR3 o.e
Sir3 binding
H3K79me3
H2AS129ph
75%
25%
Distance from ESD end (kbp)
B
YPD
30°C
5mM NAM
WT
pADH-SIR3
pTEF-SIR3
pGPD-SIR3
dot1Δ
dot1Δ pADH-SIR3
dot1Δ pTEF-SIR3
dot1Δ pGPD-SIR3
Sir3 dosage
C
30°C
30°C 5mM NAM
SGA score
H3K4R
H3K4Q
H3K4A
H3K36Q
H3K36A
H3K56A
H3K56R
H3K56Q
H3K79R
H3K79Q
H3K79A
H4K16R
H4K16Q
H4K16A
D
Chromosome III
KRR1
CDC39
SIR3 oe (NAM release)
dot1Δ SIR3 oe (NAM release)
WT (A.S.)
WT (J.S.)
WT (A.S.)
αSir3
αH3K79me
αH3K79me2
αH3K79me3
E
dot1Δ SIR3 oe (NAM release)
SIR3 oe (NAM release)
SIR3 oe (YPD)
Sir3 binding
Distance from end of E.S.D
F
SIR3 oe (NAM release), ESD excluded
dot1Δ SIR3 oe (NAM release), ESD excluded
H3K79me
H3K79me2
H3K79me3
Sir3 binding (Z-score)

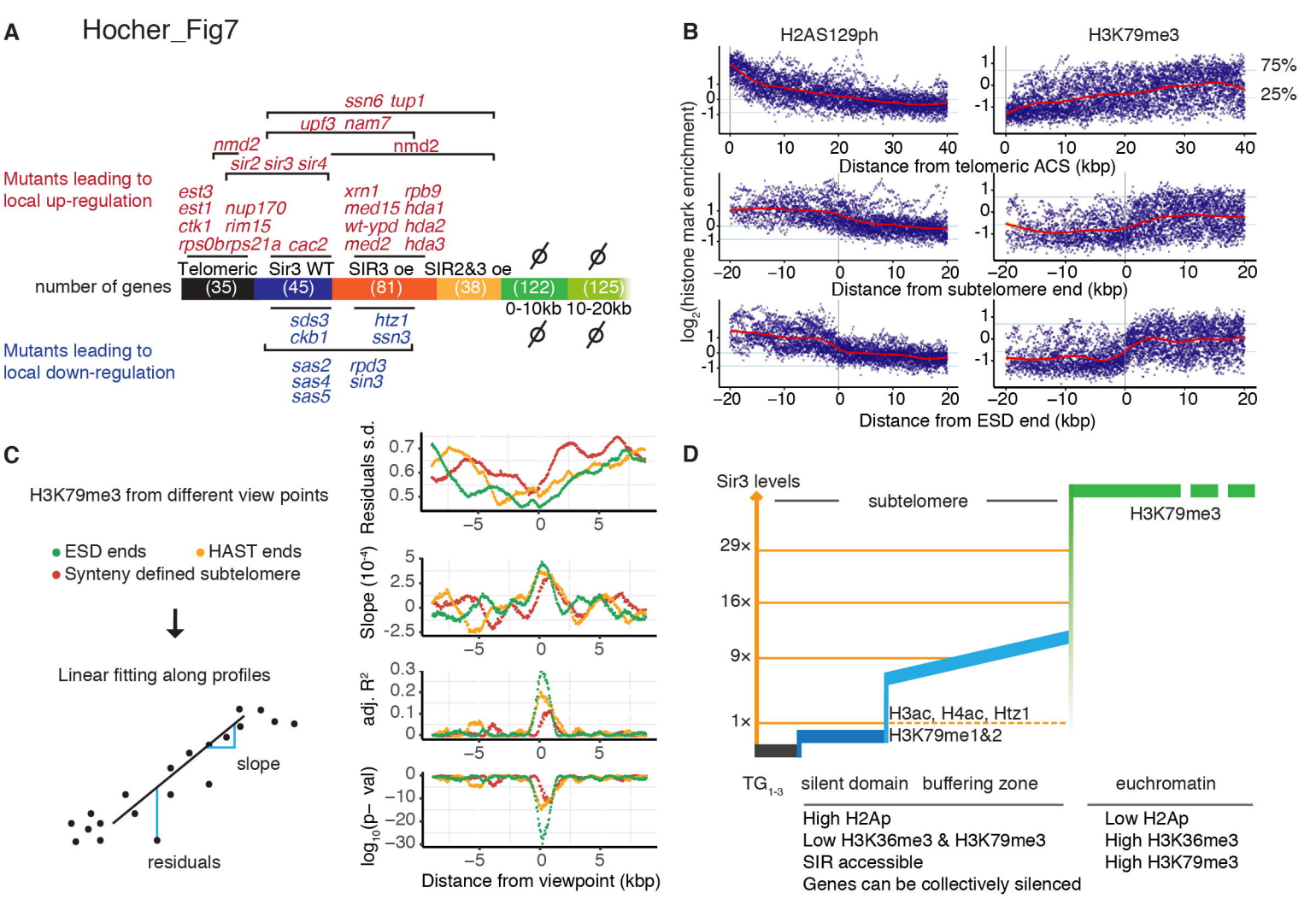
A
Hocher_Fig7
ssn6 tup1
upf3 nam7
nmd2
nmd2
sir2 sir3 sir4
Mutants leading to local up-regulation
est3
est1 nup170
ctk1 rim15
rps0b rps21a cac2
xrn1 rpb9
med15 hda1
wt-ypd hda2
med2 hda3
Telomeric
Sir3 WT
SIR3 oe
SIR2&3 oe
number of genes
(35)
(45)
(81)
(38)
(122)
(125)
0-10kb 10-20kb
sds3
ckb1
htz1
ssn3
Mutants leading to local down-regulation
sas2
sas4
sas5
rpd3
sin3
B
H2AS129ph
H3K79me3
75%
25%
log2(histone mark enrichment)
Distance from telomeric ACS (kbp)
Distance from subtelomere end (kbp)
Distance from ESD end (kbp)
C
H3K79me3 from different view points
ESD ends
HAST ends
Synteny defined subtelomere
Linear fitting along profiles
slope
residuals
Residuals s.d.
Slope (10-4)
adj. R2
log10(p- val)
Distance from viewpoint (kbp)
D
Sir3 levels
subtelomere
H3K79me3
29×
16×
9×
1×
H3ac, H4ac, Htz1
H3K79me1&2
TG1-3
silent domain
buffering zone
euchromatin
High H2Ap
Low H3K36me3 & H3K79me3
SIR accessible
Genes can be collectively silenced
Low H2Ap
High H3K36me3
High H3K79me3

SUPPLEMENTAL MATERIALS

Hocher A. et al. Expanding heterochromatin reveals discrete subtelomeric domains delimited by chromatin landscape transitions

Table of content:

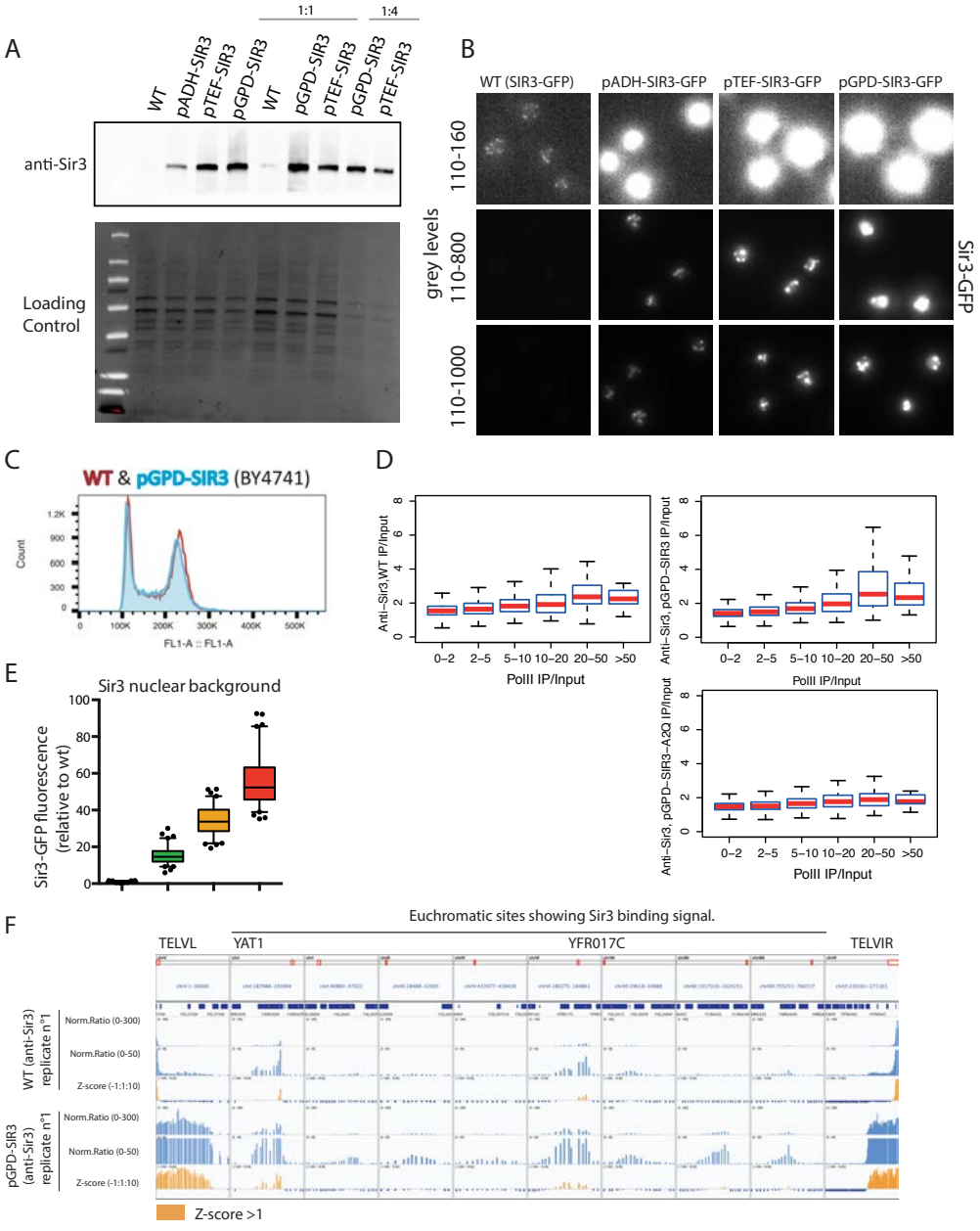
A
1:1
1:4
WT
pADH-SIR3
pTEF-SIR3
pGPD-SIR3
WT
pGPD-SIR3
pTEF-SIR3
pGPD-SIR3
pTEF-SIR3
anti-Sir3
Loading Control
B
WT (SIR3-GFP)
pADH-SIR3-GFP
pTEF-SIR3-GFP
pGPD-SIR3-GFP
grey levels
110-160
110-800
110-1000
Sir3-GFP
C
WT & pGPD-SIR3 (BY4741)
Count
FL1-A :: FL1-A
D
Anti–Sir3,WT IP/Input
Anti–Sir3, pGPD–SIR3 IP/Input
Anti–Sir3, pGPD–SIR3–A2Q IP/Input
0–2
2–5
5–10
10–20
20–50
>50
PolII IP/Input
E
Sir3 nuclear background
Sir3-GFP fluorescence (relative to wt)
F
Euchromatic sites showing Sir3 binding signal.
TELVL
YAT1
YFR017C
TELVIR
WT (anti-Sir3) replicate n°1
pGPD-SIR3 (anti-Sir3) replicate n°1
Norm.Ratio (0-300)
Norm.Ratio (0-50)
Z-score (-1:1:10)
Z-score >1

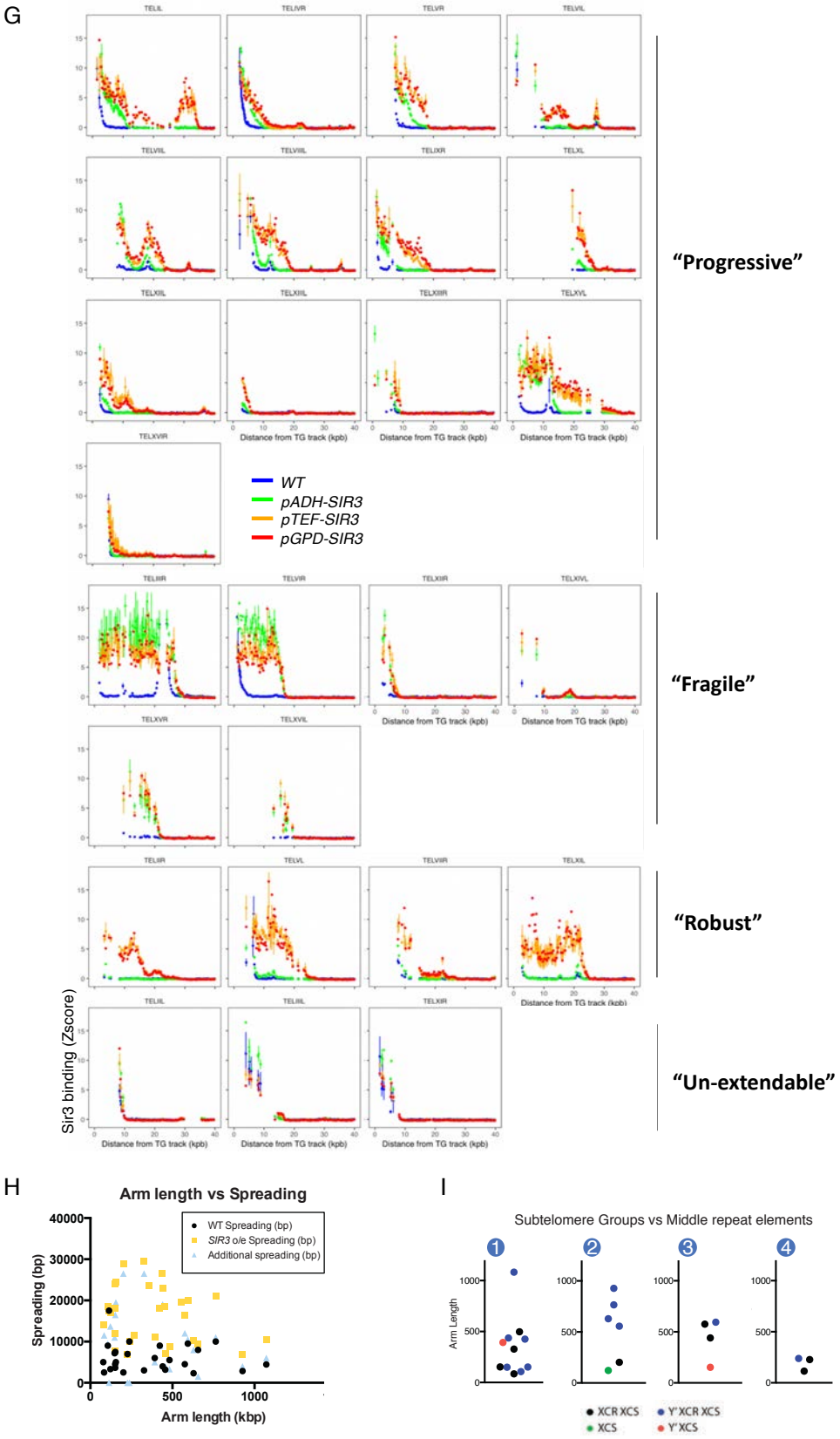

Supplemental_Fig_S1: (A) Western Blot anti-Sir3 in the strains used in Fig 1 for ChIP-chip. **(B)** Representative examples of Sir3 fluorescence in strains overexpressing Sir3-GFP. **(C)** FACS profile of

exponentially growing *WT* and *pGPD-SIR3* strains. **(D)** ChIP signal at highly expressed genes in the indicated strains. PolII enrichment data were obtained from Szilard et al. 2010. For comparison, subtelomeric binding signal is generally much higher (light blue probes at *TELVL* and *TELVI*R panel F. **(E)** Quantification of Sir3-GFP nuclear background in strains overexpressing *SIR3-GFP*. **(F)** Representative images of loci bound by Sir3 within euchromatin, light blue color indicates the probes included in Extended silent domains. Scale: 0-300. **(G)** Sir3 binding in function of Sir3 dosage at individual subtelomeres classified as in main Fig 1F. 6 subtelomeres are not shown due to insufficient data. **(H)** Chromosomal arm length versus spreading of Sir3. **(I)** Subtelomere groups as defined in Fig 1F in function of chromosomal arm length and telomeric middle repeat content.

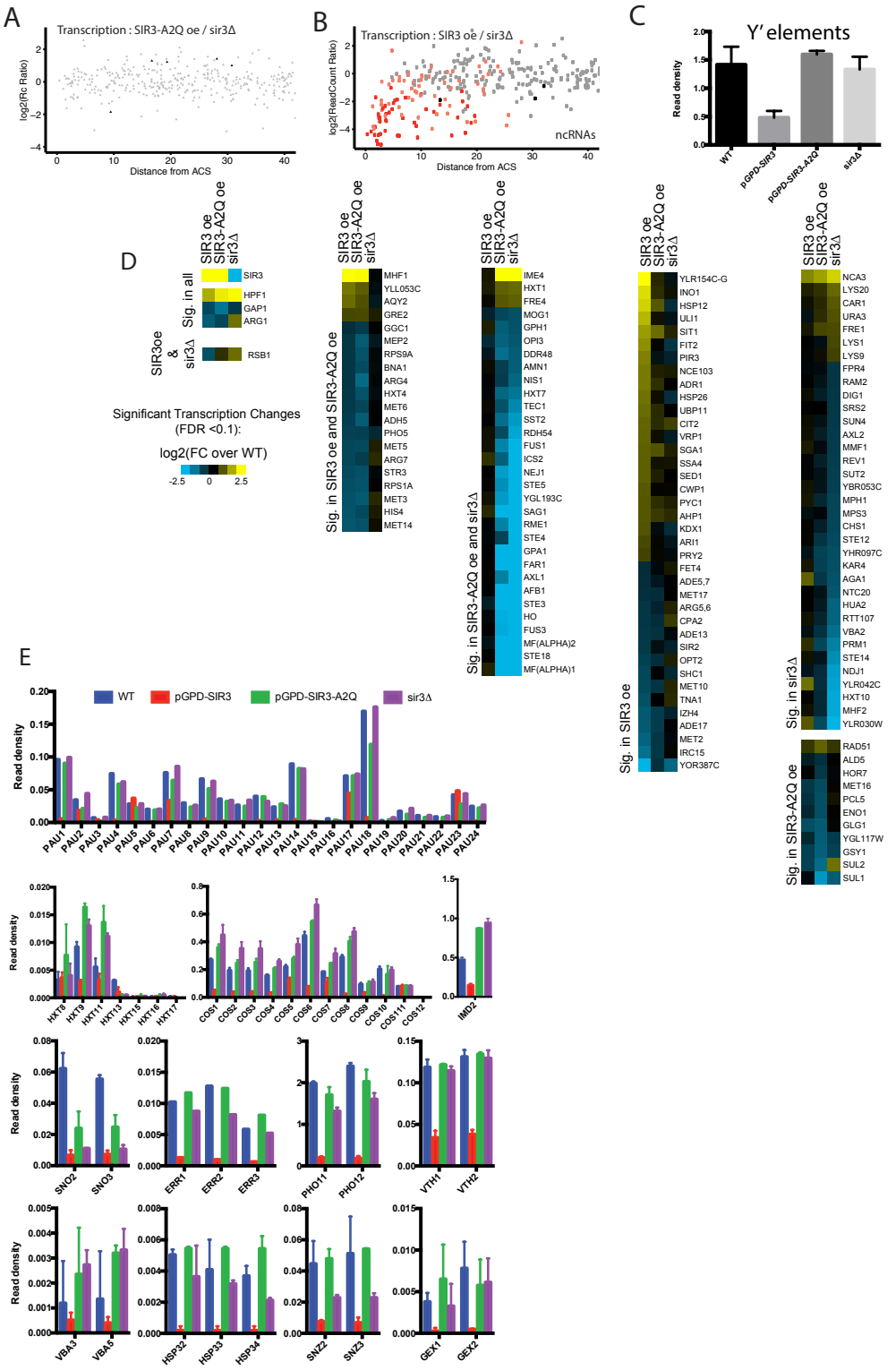

Supplemental_Fig_S2: (A) Transcriptional changes in *sir3-A2Q* mutants versus *sir3Δ* mutants. **(B)** Transcription of ncRNAs within subtelomeres, color code is identical to the main Fig 2D. **(C)** Average Read density at Y' elements. **(D)** All transcriptional changes coined significant by EdgeR within

euchromatin, color code indicates log2(FC). **(E)** Transcriptional changes of genes from subtelomeric families.

A

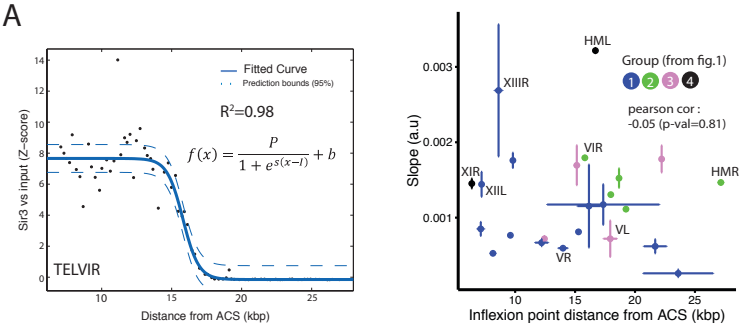

B

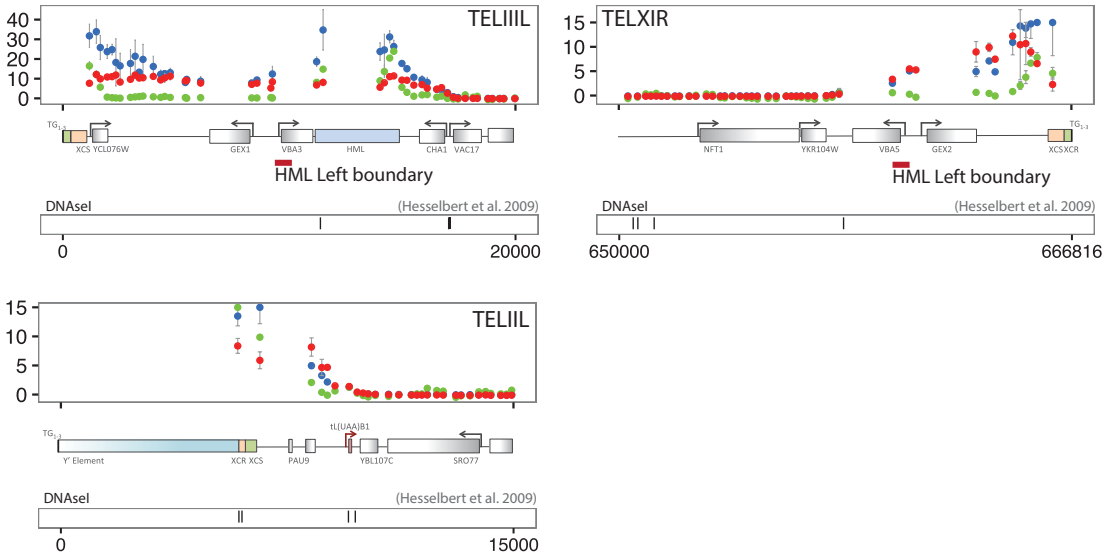

C

Transcription factor binding at extended silent domains

Transcription factor	Location			Data source
	Within E.S.D	"-1Gene"	"+1Gene"	
Abf1	3	2	2	H
Adr1	5	2	1	H
Gcn4	5	2	1	H
Hsf1	1	0	1	H
Leu3	0	0	0	H
Rap1	7	1	1	R
Reb1	3	2	2	R
|	1	0	1	H
Rgt1	0	0	0	H
Sfp1	0	0	0	H
Swi5	23 (10 Y', 3 COS)	1	0	H
Tbf1	1	2	1	P

H: Harbison et al., 2004; P: Preti et al., 2010; R: Rhee et al., 2011

Transcription factor binding at end of extended silent domains

Gene name	Gene position		Telomere	Data source
	-1	1		
YBR293W	Abf1		IIR	H
iYBR292C-1		Abf1		H
iYCR095C-0	Adr1		IIIR	H
iYCR095C-1	Gcn4			H
YCR095C	Reb1			R
YCR094W		Reb1		H;R
YDL240W		Rap1	IVL	R
YFL051C	Tbf1		VIL	P
YFL051C	Rap1			R
YFR052W		Reb1	VIR	R
iYGL254W	Abf1		VIIL	H
YGL253W		Abf1		H
YHL041W	Tbf1		VIIIL	P
YKL217W	Reb1		XIL	R
YML131W	Swi5		XIIIL	H
YMR319C		Tbf1	XIIIR	P
iYPL274W		Gcn4	XVIL	H
iYOL154W	Gcn4		XVL	H
iYOR387C-0	Adr1		XVR	H

H: Harbison et al., 2004; P: Preti et al., 2010; R: Rhee et al., 2011

Supplemental_Fig_S3: (A) Example of fitting of the ChIP-chip data, function used is shown on the graph. Right: Inferred slope versus position of inflexion point. **(B)** Examples of identified barrier at three subtelomeres at which Sir3 spreading did not extend when Sir3 dosage was increased. **(C)** Table listing transcription factor bound within ESDs or at genes neighboring ESDs Original data source is indicated.

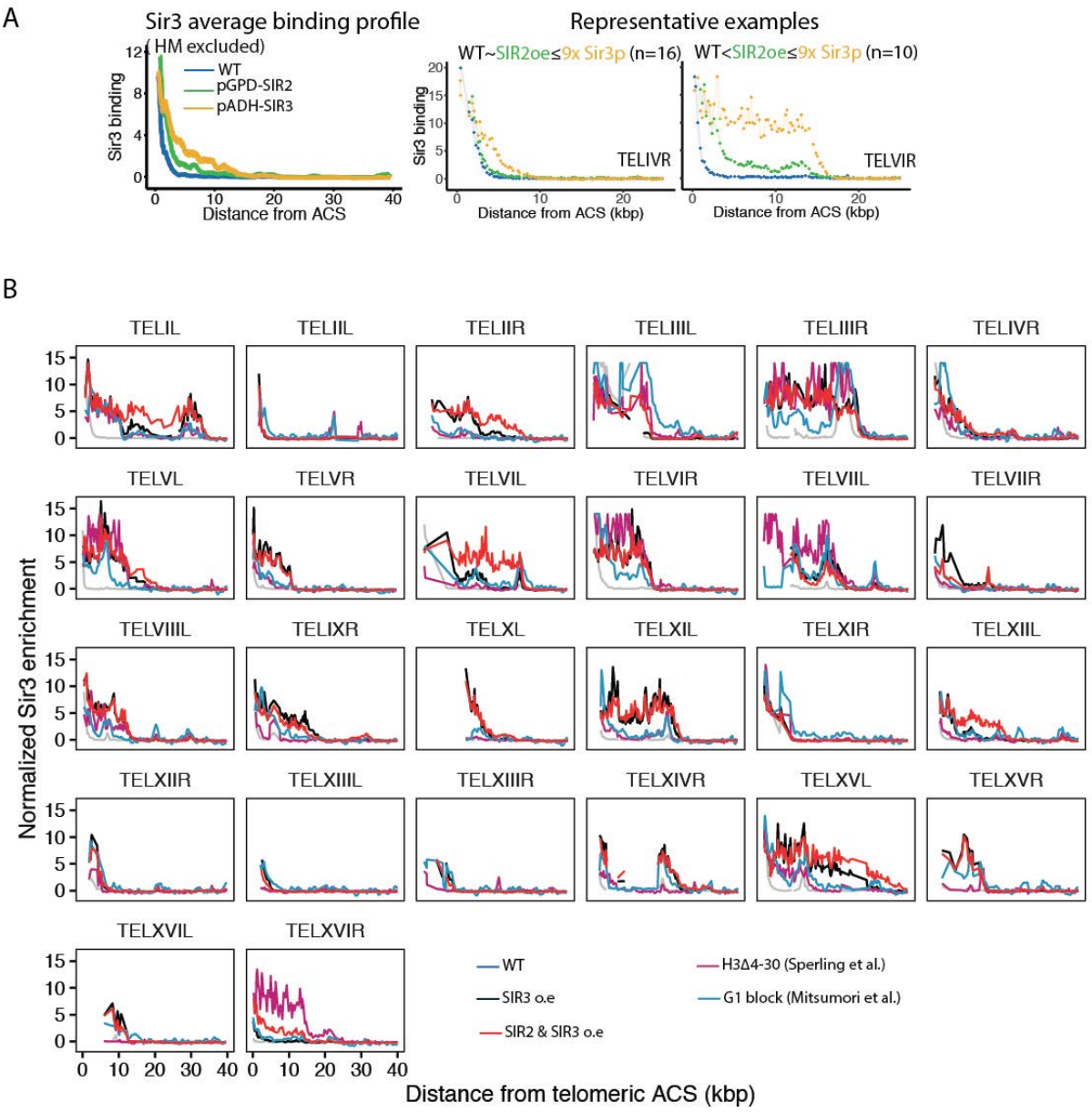

Supplemental_Fig_4: (A) Moving average of Sir3 binding at telomeres (with the exception of *TELIIIL* and *TELIIIR*, which contain *HM* loci) as in Fig 1F, in the indicated genotypes. Representative examples of Sir3 binding. **(B)** Sir3 binding at individual subtelomeres. Enrichment corresponds to standardized Sir3 binding (z-score). Origin of external dataset is indicated. 6 subtelomeres are not shown due to insufficient data.

A

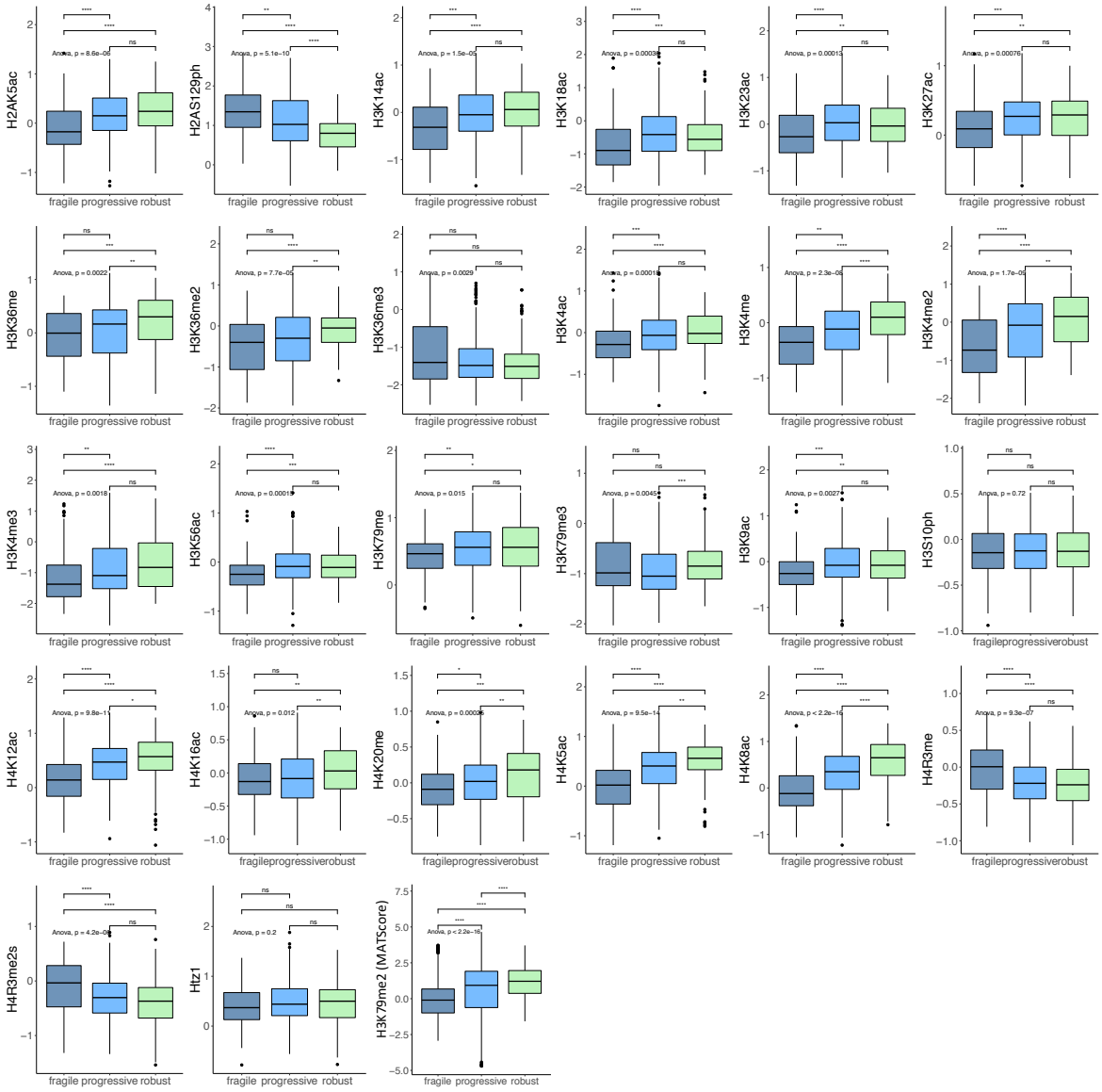
H2AK5ac
H2AS129ph
H3K14ac
H3K18ac
H3K23ac
H3K27ac
H3K36me
H3K36me2
H3K36me3
H3K4ac
H3K4me
H3K4me2
H3K4me3
H3K56ac
H3K79me
H3K79me3
H3K9ac
H3S10ph
H4K12ac
H4K16ac
H4K20me
H4K5ac
H4K8ac
H4R3me
H4R3me2s
Htz1
H3K79me2 (MATScore)
fragile progressive robust
fragileprogressiverobust
Anova, p = 8.6e-06
Anova, p = 5.1e-10
Anova, p = 1.5e-05
Anova, p = 0.00038
Anova, p = 0.00015
Anova, p = 0.00076
Anova, p = 0.0022
Anova, p = 7.7e-05
Anova, p = 0.0029
Anova, p = 0.00018
Anova, p = 2.3e-06
Anova, p = 1.7e-05
Anova, p = 0.0018
Anova, p = 0.00019
Anova, p = 0.015
Anova, p = 0.0045
Anova, p = 0.0027
Anova, p = 0.72
Anova, p = 9.8e-11
Anova, p = 0.012
Anova, p = 0.00036
Anova, p = 9.5e-14
Anova, p < 2.2e-16
Anova, p = 9.3e-07
Anova, p = 4.2e-06
Anova, p = 0.2
Anova, p < 2.2e-16

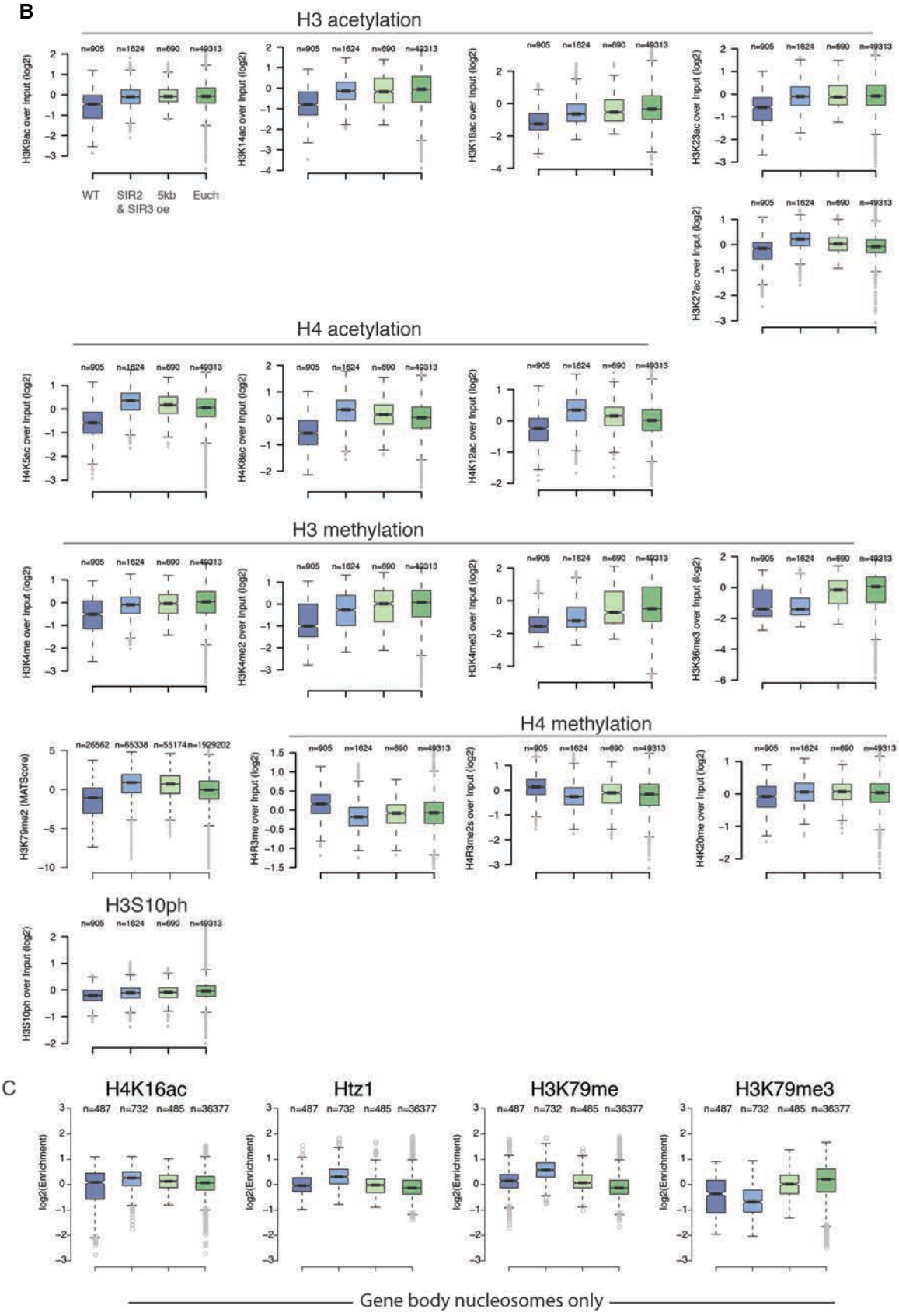
B
H3 acetylation
H3K9ac over Input (log2)
H3K14ac over Input (log2)
H3K18ac over Input (log2)
H3K23ac over Input (log2)
H3K27ac over Input (log2)
n=905 n=1624 n=690 n=49313
WT
SIR2 & SIR3 oe
5kb
Euch
H4 acetylation
H4K5ac over Input (log2)
H4K8ac over Input (log2)
H4K12ac over Input (log2)
H3 methylation
H3K4me over Input (log2)
H3K4me2 over Input (log2)
H3K4me3 over Input (log2)
H3K36me3 over Input (log2)
H3K79me2 (MATScore)
n=26562 n=65338 n=55174 n=1929202
H4 methylation
H4R3me over Input (log2)
H4R3me2s over Input (log2)
H4K20me over Input (log2)
H3S10ph
H3S10ph over Input (log2)
C
H4K16ac
Htz1
H3K79me
H3K79me3
n=487 n=732 n=485 n=36377
log2(Enrichment)
Gene body nucleosomes only

Supplemental_Fig_S5: (A) Distribution of selected histone marks relative to H3 (data from Weiner et al. 2015, except H3K79me2 from Schulze et al. 2009) at the flanks of WT silent domain ends (5kb) at the three groups of subtelomeres that are eventually sensitive to *SIR3* overexpression. **(B)** Distribution of selected histone marks relative to H3 (data from Weiner et al. 2015 except H3K79me2, from Schulze et al. 2009) along wild type silenced domains and within the contiguous subtelomeric domains accessible to Sir3 upon overexpression. As a control, the distribution of those marks within the 5 kb contiguous to the end of extended silent domains as well as the genome wide distribution of those. **(C)** Identical as B but focusing on nucleosomes localized over gene bodies.

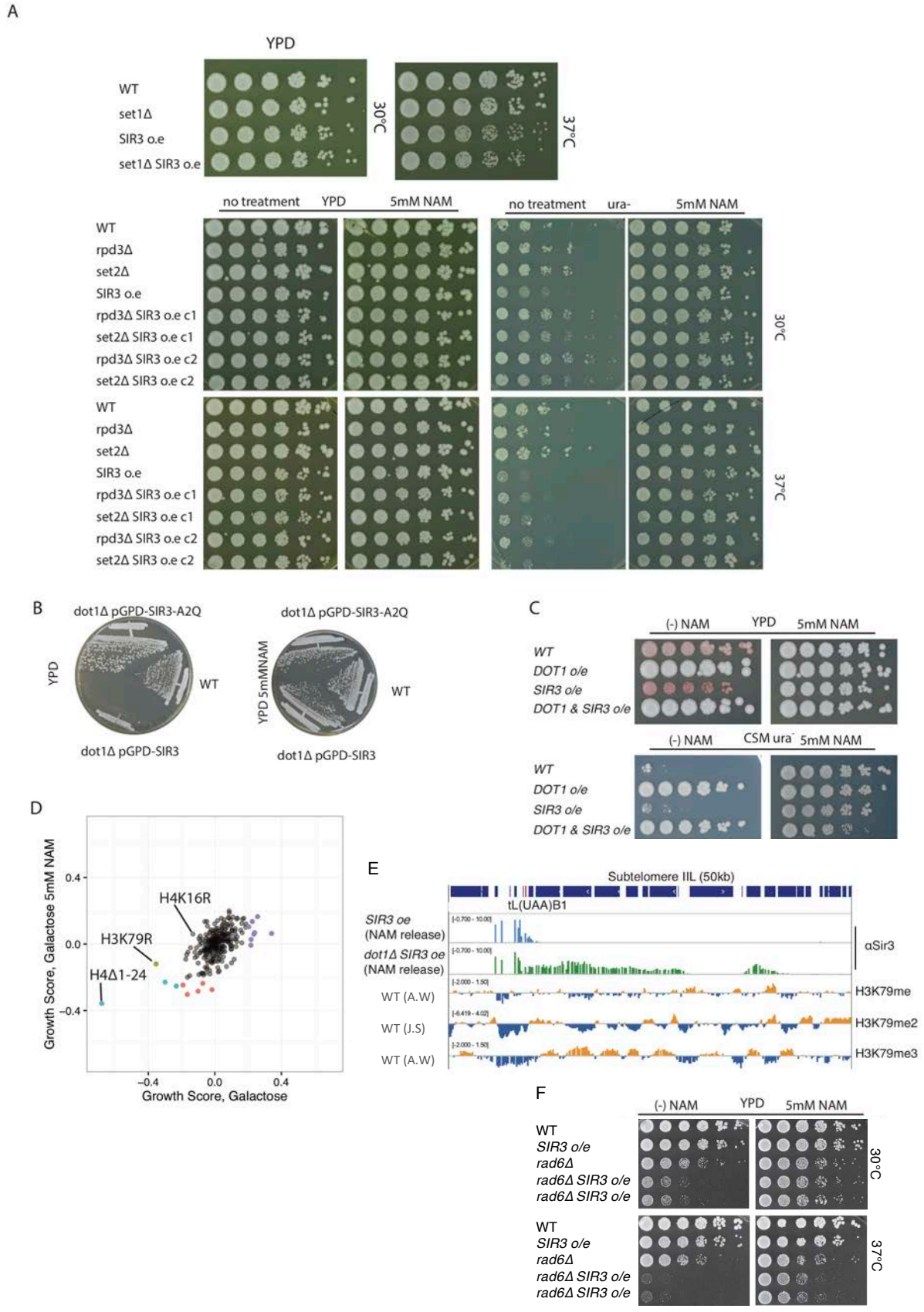

Supplemental_Fig_S6: (A) Drop assays probing viability in the presence or absence of 5 mM NAM. Protocol is identical to the one of Fig 6B. Genotypes are as indicated. **(B)** *dot1* mutants overexpressing

Sir3-A2Q are viable. **(C)** *DOT1* overexpression counteracts *SIR3* overexpression. WT strains have an *ADE2* reporter gene located at telomere VL. **(D)** SGA score of all histone point mutants probed, colored points pass our significance criterion and are colored according to their respective behavior (rescued by NAM treatment, sick in all conditions). **(E)** Genome browser visualization of Sir3 binding in *pGPD-SIR3* and *dot1Δ pGPD-SIR3* strains 8 hours after being released from 5 mM NAM. *tRNA tL(UAA)B1* is labelled in red. H3K79 methylation enrichment were obtained from Weiner et al. 2015 for H3K79me and H3K79me3 and from Schulze et al. 2009 for H3K79me2 (Mat score is shown). **(F)** Drop assays probing viability in the presence or absence of 5 mM NAM in *rad6* mutants. Cells were grown over night in YPD + 5 mM NAM and release 3h in YPD before plating on YPD or YPD + NAM.

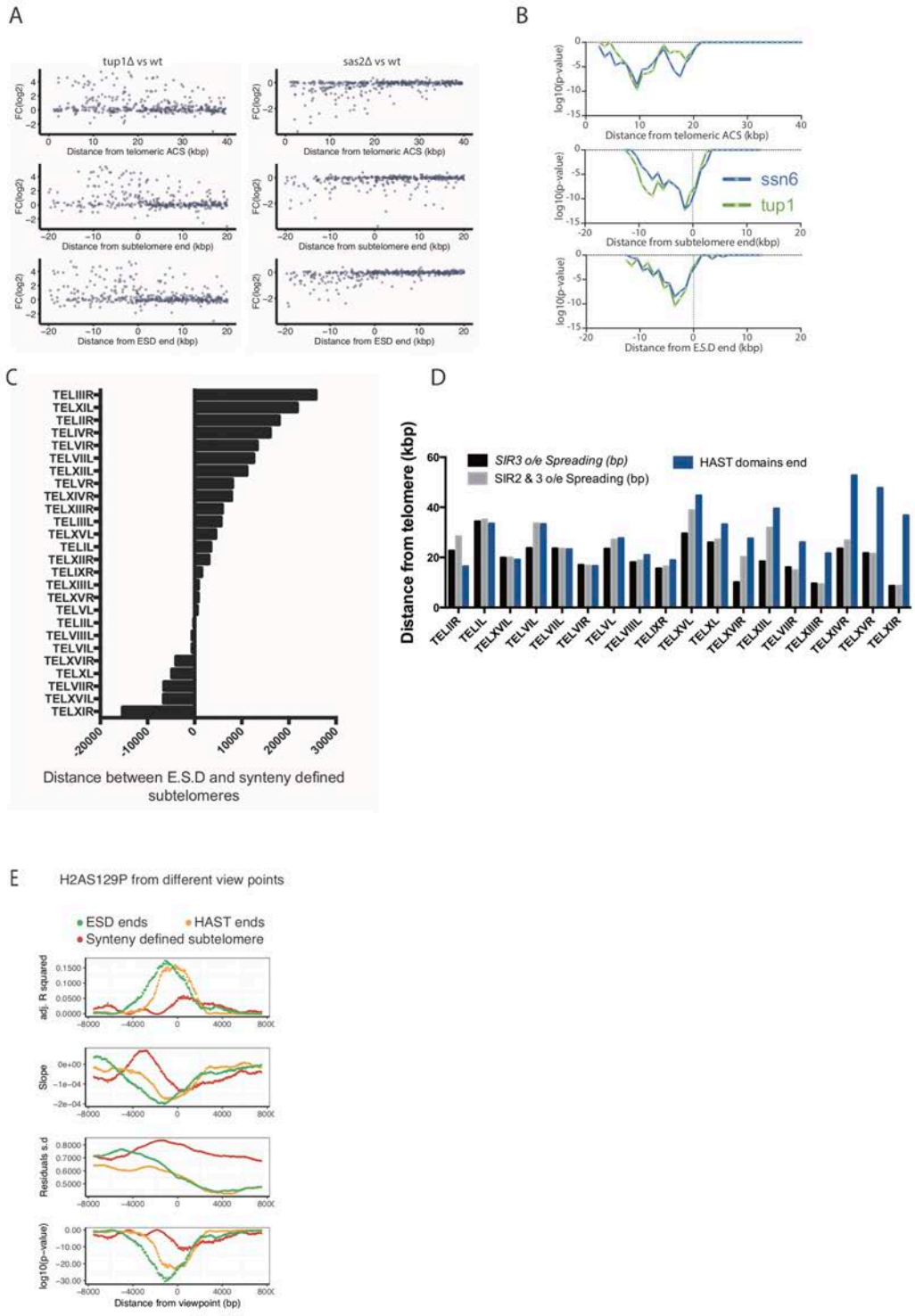

Supplemental_Fig_S7: (A) Expression changes in the *tup1* and *sas2* mutants in function of different subtelomeric viewpoints. **(B)** Corrected p-values of hyper-geometric test for sliding 5 kb windows (step=1kb) is shown for *tup1* and *ssn6* mutants in function of different subtelomeric viewpoints. This analysis corresponds to Fig 7B. Each point represents the center of a 5 kb window. **(C)** Comparison of ESD ends with subtelomere ends as defined by synteny in Yue et al. 2017. **(D)** Comparison of ESD ends with HAST domain ends as defined in Robyr et al. 2002. **(E)** H2AS129ph transitions at subtelomeres in function of different viewpoints, similar to Fig 7C.

#Supplemental_Table_S1
#List of detected binding sites of Sir3 within euchromatin. All non-subtelomeric Sir3 binding s

	Coordinates				
Site #	Chromosome	Start	Stop	Flanking gene(s)	Type
1	chrI	44488	45151	YAL053W	Intergene
1	chrI	44488	45151	YAL054C	Intergene
2	chrI	189742	192296	YAR035W	Gene body
3	chrII	428552	428610	YBR092C	Gene body
4	chrIII	30013	30532	YCL054W	Intergene
4	chrIII	30013	30532	YCL055W	Intergene
5	chrIII	50934	52028	YCL040W	Gene body
6	chrIV	436567	436626	-	Flanks 2 tRNAs
7	chrIV	1430227	1430284	YDR488C	Gene body
8	chrVI	181554	184062	YFR017C	Gene body
8	chrVI	181554	184062	YFR018C	Gene body
9	chrVIII	175722	175767	YHR033W	Gene body
10	chrX	360277	360518	YJL043W	Gene_body
11	chrX	683821	683880	YJR137C	Intergene
11	chrX	683821	683880	YJR138W	Intergene
12	chrXI	68881	68932	YKL198C	Gene body
13	chrXII	1012859	1012911	YLR438W	Gene body
14	chrXII	1020034	1022147	YLR442C	Gene body
15	chrXIII	757329	758041	YMR244W	Gene body
16	chrXIV	25008	25466	YNL327W	Gene body
17	chrXV	480828	480875	YOR084W	Gene body
18	chrXVI	520221	520280	YPL016W	Intergene
18	chrXVI	520221	520280	IRC15	Intergene

sites (n=18) (defined as euchromatic site at which at least two neighbouring probes are bou

RNA levels and Significance

log2(Mutant/WT)			**False Discovery Rate (EdgeR)**	
SIR3 oe vs WT	*SIR3-A2Q oe vs WT*	*sir3 vs WT*	*SIR3 oe vs WT*	*SIR3-A2Q oe vs WT*
0,1	0,0	-0,1	n.s	n.s
0,3	-0,1	-0,2	n.s	n.s
-0,4	0,2	0,2	n.s	n.s
0,3	-0,1	-0,2	n.s	n.s
0,1	0,1	-0,4	n.s	n.s
0,2	-0,9	-1,1	n.s	n.s
-0,4	-0,9	-0,1	n.s	n.s
-	-	-	-	-
0,2	-0,1	-0,4	n.s	n.s
-0,7	-0,7	0,1	n.s	n.s
-0,2	0,4	0,2	n.s	n.s
0,0	0,3	0,2	n.s	n.s
-1,3	-0,1	-0,6	n.s	n.s
-1,0	-1,0	0,3	4,2E-04	6,7E-04
0,0	0,1	0,1	n.s	n.s
0,0	-0,1	-0,2	n.s	n.s
0,2	0,1	0,7	n.s	n.s
4,7	4,8	-3,6	1,5E-81	1,6E-85
-0,9	0,2	-0,2	n.s	n.s
0,1	0,0	-0,1	n.s	n.s
-0,1	0,4	0,1	n.s	n.s
-0,1	0,0	0,1	n.s	n.s
-1,6	-0,8	0,1	4,0E-02	n.s

nd (z-score >0.5) by Sir3 upon overexpression of SIR3) together with the change in transcript l

	Sir3 binding this study				**Sperling et al.**
sir3 vs WT	*WT*	*pADH-SIR3*	*pTEF-SIR3*	*pGPD-SIR3 (W303)*	*H3Δ4-30*
n.s	no	1of2	yes	yes	yes
n.s	no	1of2	yes	yes	yes
n.s	yes	yes	yes	yes	yes
n.s	no	yes	yes	yes	no
n.s	no	no	no	yes	yes
1,8E-02	no	no	no	yes	yes
n.s	no	yes	yes	yes	yes
-	no	1of2	yes	yes	yes
n.s	yes	yes	yes	yes	yes
n.s	yes	yes	yes	yes	yes
n.s	yes	yes	yes	yes	yes
n.s	1of2	1of2	no	yes	yes
n.s	1probeonly	1of2	no	1of2	yes
n.s	yes	yes	yes	yes	yes
n.s	yes	yes	yes	yes	yes
n.s	1of2	yes	yes	yes	yes
n.s	1of2	yes	yes	yes	yes
7,0E-45	no	no	yes	yes	no
n.s	1of2	yes	yes	yes	yes
n.s	no	no	yes	yes	no
n.s	no	1of2	no	yes	yes
n.s	1of2	yes	yes	yes	yes
n.s	1of2	yes	yes	yes	yes

levels (read density) for the flanking genes in WT versus SIR3 overexpressing or SIR3 dele

Mitsumori et al.

G1	Extended upon oe
CN1	
CN17	
CN4	no
CN7	yes
CN7	yes
CN11	no
CN11	no
	no
	yes
CN25	
	oneprobe
	oneprobe

ɛted strains.

#Supplemental table 2: yeast strains use

ID	Mating T.
191	alpha
1254	alpha
1256	alpha
2487	a
2627	a
2629	a
2554	a
1667	a
1668	a
779	a
3441	a
3442	a
3443	a
2056	a
2986	a
2987	a
2476	a
3004	alpha
3123	alpha
3180	alpha
3181	alpha
3182	alpha
3183	alpha
3184	alpha
2838	alpha
2841	alpha
3301	1N
3333	1N

d in this study.

genotype
ade2-1::ADE2 adh4::URA3-4xUASG-(C1-3A)n ppr1Δ::HIS3
rap1::GFP-RAP1(LEU2)
ade2-1::ADE2 adh4::URA3-4xUASG-(C1-3A)n ppr1Δ::HIS3
rap1::GFP-RAP1(LEU2) sir3::GPD-SIR3(NAT)
ade2-1::ADE2 adh4::URA3-4xUASG-(C1-3A)n ppr1Δ::HIS3
rap1::GFP-RAP1(LEU2) sir3::GPD-sir3-A2Q(NAT)
ade2-1::ADE2 hmlΔ::HPH rap1::RAP1-GFP(LEU2)
ade2-1::ADE2 hmlΔ::HPH rap1::RAP1-GFP(LEU2) sir3::pADH-SIR3(NAT)
ade2-1::ADE2 hmlΔ::HPH rap1::RAP1-GFP(LEU2) sir3::pTEF-SIR3(NAT)
ade2-1::ADE2 hmlΔ::HPH rap1::RAP1-GFP(LEU2) sir3::GPD-Sir3(NAT)
RAD5+ rap1::RAP1-GFP(LEU2) RDN1::ADE2 sir2::GPD-SIR2(KanMX)
RAD5+ rap1::RAP1-GFP(LEU2) RDN1::ADE2 sir2::GPD-SIR2(KanMX)sir3::GPD-SIR3(NAT)
ade2-1::ADE2 sir3::SIR3-GFP(LEU2)
ade2-1::ADE2 sir3::(KAN) pADH-SIR3-GFP(LEU2)
ade2-1::ADE2 sir3::(KAN)pTEF-SIR3-GFP(LEU2)
ade2-1::ADE2 sir3::(KAN) pGPD-SIR3-GFP(LEU2)
can1::MFA1pr-HIS3 hht1-hhf1::NatMX4 hht2-hhf2::[HHTS-HHFS]*-URA3 where H4WT
can1::MFA1pr-HIS3 hht1-hhf1::NatMX4 hht2-hhf2::[HHTS-HHFS]*-URA3 where H3Δ4-30 Rap1-GFP(LEU2)
can1::MFA1pr-HIS3 hht1-hhf1::NatMX4 hht2-hhf2::[HHTS-HHFS]*-URA3 where H3Δ4-30 Rap1-GFP(LEU2) pGPD-SIR3(NAT)
rap1::GFP-RAP1(LEU2) sir3::GPD-SIR3(NAT)
ade2-1::ADE2 adh4::URA3-4xUASG-(C1-3A)n ppr1Δ::HIS3
rap1::GFP-RAP1(LEU2) bre1Δ::KanMx
ade2-1::ADE2 adh4::URA3-4xUASG-(C1-3A)n ppr1Δ::HIS3
rap1::GFP-RAP1(LEU2) bre1Δ::KanMx SIR3::pGPD-SIR3 (NatMx)
ade2-1::ADE2 adh4::URA3-4xUASG-(C1-3A)n ppr1Δ::HIS3
rap1::GFP-RAP1(LEU2) dot1Δ::KanMx
ade2-1::ADE2 adh4::URA3-4xUASG-(C1-3A)n ppr1Δ::HIS3
rap1::GFP-RAP1(LEU2) set1Δ::KanMx
ade2-1::ADE2 adh4::URA3-4xUASG-(C1-3A)n ppr1Δ::HIS3
rap1::GFP-RAP1(LEU2) dot1Δ::KanMx pGPD-SIR3-A2Q (NAT)
ade2-1::ADE2 adh4::URA3-4xUASG-(C1-3A)n ppr1Δ::HIS3
rap1::GFP-RAP1(LEU2) dot1Δ::KanMx pGPD-SIR3 (NAT)
ade2-1::ADE2 adh4::URA3-4xUASG-(C1-3A)n ppr1Δ::HIS3
rap1::GFP-RAP1(LEU2) set1Δ::KanMx pGPD-SIR3(NAT)
ade2-1::ADE2 adh4::URA3-4xUASG-(C1-3A)n ppr1Δ::HIS3
rap1::GFP-RAP1(LEU2) rpd3Δ::KanMx
ade2-1::ADE2 adh4::URA3-4xUASG-(C1-3A)n ppr1Δ::HIS3
rap1::GFP-RAP1(LEU2) rpd3Δ::KanMx pGPD-SIR3(NAT)
ade2-1::ADE2 adh4::URA3-4xUASG-(C1-3A)n ppr1Δ::HIS3
rap1::GFP-RAP1(LEU2) set2Δ::(KanMx)
ade2-1::ADE2 adh4::URA3-4xUASG-(C1-3A)n ppr1Δ::HIS3
rap1::GFP-RAP1(LEU2) set2Δ::(KanMx) sir3::GPD-SIR3(NAT)

background
(W303)
(W303)
(W303)
(W303)
(W303)
(W303)
(W303)
(W303)
(W303)
(W303)
(W303)
(W303)
BY4733
BY4733
BY4733
BY4741
(W303)
(W303)
(W303)
(W303)
(W303)
(W303)
(W303)
(W303)
(W303)
(W303)
(W303)